ELSEVIER

Journal of Volcanology and Geothermal Research 114 (2002) 391–417

Journal of volcanology and geothermal research

www.elsevier.com/locate/jvolgeores

Applications of autoregressive models and time–frequency analysis to the study of volcanic tremor and long-period events

Philippe Lesage [a,*], François Glangeaud [b], Jérôme Mars [b]

[a] *Laboratoire de Géophysique Interne et Tectonophysique, Université de Savoie, 73376 Le Bourget-du-Lac, France*
[b] *Laboratoire des Images et des Signaux, Institut National Polytechnique de Grenoble, Grenoble, France*

Received 9 August 2000; received in revised form 27 July 2001; accepted 27 July 2001

Abstract

Volcanic tremor and long-period (LP) events are characterized by sharp spectral peaks that generally result from resonance effects at the source and which concentrate most of the radiated energy. The understanding of these seismovolcanic phenomena requires good descriptions of the distribution in time and frequency of the different spectral components included in the signals, as well as a separation of the resonance effects from less energetic effects such as excitation and propagation. We address the issue of extracting from individual records information as detailed as possible on the physical processes involved at the source. We introduce and compare several time–frequency analysis methods, and we describe the application of autoregressive modeling and deconvolution methods to the characterization and separation of the main spectral components. We propose a signal analysis approach based on the joint use of a set of complementary methods, and we present applications to several examples of volcanic tremor and LP events. The time–frequency analysis of some of the LP events taken as examples reveals short-duration components at the seismogram onsets with energy concentrated at frequencies either higher or lower than the main resonance frequencies. These seismic phases are probably related to the excitation processes of the volcanic resonators. In several cases, the arrival of the main spectral peak has a delay of a few tenths of a second with respect to the first arrival. The residual signals obtained by deconvolving and eliminating the main spectral components contain information about the excitation, such as duration, delay, or frequency band. The residual signals are short for LP events, and continuous for volcanic tremor. The autoregressive modeling of the sample records gives precise estimations of the frequency and quality factor of the main spectral peaks. The measured parameters cover a wide range of values, which is consistent with the great variety of fluids filling resonating cavities in volcanoes.

Keywords: seismology; volcano; volcanic tremor; long-period event; signal processing

1. Introduction

Volcanic tremor and long-period (LP) events are the most distinctive features of the seismic activity of volcanoes. They are thought to be di-

* Corresponding author. Fax: +33-4-79-75-87-42.
E-mail address: lesage@univ-savoie.fr (P. Lesage).

0377-0273/02/$ – see front matter
PII: S0377-0273(01)00298-0

rectly related with physical processes that arise in magmatic or hydrothermal systems, and involve fluids such as magma, water, gas or vapor filling cavities such as magma chamber, or conduits and cracks (see Chouet, 1996a,b for a review). Their frequent observation prior to volcanic eruptions and their close relationship with the triggering mechanisms of eruptions make their study crucial for improving eruption forecasting (e.g., Chouet et al., 1994). It is thus important to understand the physical phenomena involved at their sources. LP event and tremor records are generally characterized by emergent first arrival and the lack of a clear shear-wave, which makes classical methods of seismic analysis, such as hypocenter localization, inoperative. Their spectra usually contain one or several narrow peaks, sometimes regularly spaced, which allow easy identification of this kind of event among volcano-tectonic earthquakes. There is now a large consensus for interpreting most of the spectral peaks as resonance phenomena at the source. Nevertheless, path or site effects may be important, especially when source resonances are weak (Gordeev, 1993; Kedar et al., 1998; Lesage et al., 1999; Mora et al., 2001). LP events and tremor seem to share common source processes and location. They differ mainly in the duration of vibrations, which may reflect differences in durations of the excitation processes.

Source modeling splits into two aspects. First, many models describe the resonance of fluid-filled cavities with various geometries such as (1) sphere (Crosson and Bame, 1985; Fujita et al., 1995); (2) pipe (Chouet, 1985; Garcés and McNutt, 1997); or (3) crack (Aki et al., 1977; Chouet, 1981, 1986, 1988). The resonance modes of the cavities are related to the acoustic properties of fluid and rock, the geometry and size of the cavity, and the coupling between acoustic waves in the fluid and elastic waves in the rock. Second, other studies have suggested various mechanisms of oscillation excitation, including unsteady fluid flow (Ferrick et al., 1982; Julian, 1994; Morrissey and Chouet, 1997), hydrothermal boiling (Leet, 1988; Kedar et al., 1998), or the collective oscillation of bubble clouds (Lu et al., 1990; Yoon et al., 1991; Chouet, 1996b). Among the great variety of complex mechanisms proposed to explain LP events and tremor, the choice of a model adapted to a specific case should be guided both by the state of knowledge of the volcano under study, including geological and geophysical data, and by information obtained from seismic observations.

This leads to the issue of extracting useful information from seismic signals. For this purpose, a first domain of investigation is the estimation of the spectral content of the records, i.e., the distribution of energy with respect to frequency and time. This includes a characterization of the spectral peaks, namely, their frequency, phase, width, amplitude, stability, arrival time, and duration. This can be obtained by using various spectral estimators and time–frequency analysis methods based on the classical Fourier transform, the parametric modeling of time series, or on other methods such as wavelet transform (Kay and Marple, 1981; Marple, 1987; Flandrin et al., 1992). A second aim of signal processing is to extract or enhance some important features of the records. As most of the tremor and LP event energy is concentrated in sharp spectral peaks, the corresponding harmonic components usually conceal less energetic parts of the signal, including low-amplitude arrivals or transients, which often have spread spectra. It is thus necessary to eliminate the main harmonic components by using adapted filters, deconvolution or spectral whitening methods.

From a signal analysis point of view, the observed seismic signal $x(t)$ may be considered as the convolution product of the impulse response of the resonator $r(t)$ with the excitation function $e(t)$ and the propagation and site effects $p(t)$, plus additive noise $n(t)$:

$$x(t) = e(t) \cdot^{*} r(t) \cdot^{*} p(t) + n(t)$$

The sharp spectral peaks generally result from the resonator term $r(t)$ and, to a lesser extent, from site effects described by $p(t)$. The function $r(t)$ is composed of a superposition of decaying complex exponential functions, which correspond to the normal modes of the resonator. These functions are solutions of second-order linear differ-

ential equations, the coefficients of which are related to the physical features of the resonator. Because of the equivalence between a linear differential equation and a linear difference equation, autoregressive (AR) methods are well suited to the analysis of this kind of signal. AR methods consider a discrete time series $x(t)$ as the response of a linear AR (or infinite impulse response) filter. The poles of the filter correspond to the complex eigen-frequencies of the resonator. Thus AR models provide direct basic information on the physical system. In seismological applications, AR models have been used by several authors under different versions and names, such as Prony's method (Feng Chao and Gilbert, 1980), maximum entropy spectral analysis (Seidl et al., 1990), or Sompi method (Fukao and Suda, 1989; Nakano et al., 1998). Once the AR filter coefficients are obtained from a signal $x(t)$, it is possible to calculate the inverse filter and deconvolve the resonance effect from the observed data (Nakano et al., 1998). This operation is especially well suited for harmonic tremor and LP events which contain only one spectral peak. In this case, the deconvolved residue is closely related to the excitation function of the resonator and thus contains valuable information on the driving process at the source. Nevertheless, it is important to note that the problem of decomposing a signal into the convolution product of several terms has an infinite number of solutions. Thus, some assumptions or independent information must be used in order to better constrain the problem.

In this paper, we propose an approach of seismic signal analysis based on the joint use of various complementary methods. We start with a brief presentation of several signal processing methods, including AR modeling and deconvolution, spectral whitening and time–frequency analysis such as short-time Fourier transform, continuous wavelet transform, or Capon and Lagunas methods. We apply these methods to a small set of volcanic tremor and LP events and specify their limitations and emphasize their main potentialities to provide pertinent information for the development of physical models.

2. Methods

A wide range of signal processing methods can be applied to the analysis of volcanic seismic events. It is interesting to use a combination of several methods because (1) these generally yield complementary results, (2) a given method may or may not produce useful information depending on the signal considered, and (3) spurious results obtained by one method may be identified by using other algorithms.

2.1. Fourier spectrum

Estimations of the power spectral density (PSD) based on the Fourier transform are widely used and their properties are extensively discussed in most signal processing books (see e.g., Kay and Marple, 1981). A very common PSD estimator is the squared Fourier transform modulus, or Fourier spectrum. However, it must be pointed out that this estimator can be biased, and that a resonance frequency in a signal does not always coincide with the frequency of the maximum of the corresponding spectral peak (Mari et al., 1998, p. 405). The use of either averaged periodograms or smoothed spectra usually improves the estimation of the frequencies. The Fourier transform gives information about the frequency content of a signal, but does not provide the location of these frequencies in the time domain. Many methods have been developed in order to describe processes with time varying frequencies (Flandrin et al., 1992). Some of these methods are discussed in the following sections.

2.2. Short-time Fourier transform, or windowed Fourier transform, or spectrogram

Time localization can be obtained by windowing the data at different times with sliding window functions $g(t)$ (Harris, 1978). The Fourier transform of this procedure applied on a signal $x(t)$ is called short-time Fourier transform (STFT), or spectrogram. It is defined as:

$$\mathrm{STFT}_x^{(g)}(t,f) = \int_{t'} [x(t')\cdot g^*(t-t')]\exp(-2i\pi f t')\mathrm{d}t'$$

where g^* is the complex conjugate of g. The STFT at a given time t is the Fourier transform of the signal $x(t')$ multiplied by a shifted analysis window $g^*(t-t')$ centered on t. The STFT can be seen as a local spectrum of the signal $x(t')$ around the analysis time t. The result of such Fourier transform is significantly influenced by the choice of the analysis window and by its length. It is clear that a good time resolution of the STFT requires a narrow window in time. In contrast, a good frequency resolution of the STFT requires a narrow filter in the frequency domain (respectively, a large window in time). Unfortunately, Heisenberg's uncertainty principle prohibits the existence of a window with arbitrarily small duration and small bandwidth. It is well known that once a window function $g(t)$ is chosen, both time and frequency resolutions are fixed. This means that for any given t and f, the frequency resolution in time is fixed, and the entire phase space is uniformly described by cells of fixed sizes. Thus, the STFT is inadequate for the study of signals with different size features because it is not possible to design an optimal window for analyzing the process.

2.3. The continuous wavelet transform

Since the concept of wavelet transform was first formalized by Morlet (Morlet et al., 1982), a huge number of works have been published in this domain (Goupillaud et al., 1984; Mallat, 1989; Meyer, 1989; Daubechies, 1990). The wavelet transform overcomes some limitations of the STFT and can give a more accurate time–frequency description of signals containing low- and high-frequency components. In this transform, the time–frequency space is divided in non-uniform size cells. This is achieved by using analyzing functions called wavelets, which are characterized by two parameters, the translation parameter as in the STFT, and the dilatation parameter. When these parameters take continuous values, the operation is called continuous wavelet transform (CWT). It is defined in the time frequency domain as:

$$\mathrm{CWT}_x^{(g)}(t,f) = \sqrt{\frac{f}{f_0}} \cdot \int_{t'} x(t') \cdot g^* \left(\frac{f}{f_0}(t-t') \right) \cdot \mathrm{d}t'$$

where $g(t)$ is the analyzing wavelet, which is a real or complex band-pass function centered at $t=0$ in the time domain. The dilatation parameter f_0 is equal to the center frequency of $g(t)$. Originally, the wavelet transform was introduced as a time scale representation (Daubechies, 1990; Mallat, 1989; Meyer, 1989), thus the classical formulation can be retrieved from the time–frequency formulation by taking the analysis scale a as $a=f_0/f$. The choice of the wavelet $g(t)$ is neither unique nor arbitrary. It must be a zero-mean function with unit energy and compact support (i.e., with sufficiently fast decay) to obtain localization in time. Among the many available wavelets, the Morlet wavelet has been widely used in geophysics. It is a complex wavelet, which is able to extract information on both the amplitude and phase. The Morlet wavelet is defined by:

$$g(t) = (\pi t_0)^{-\frac{1}{4}} \exp\left[-\frac{1}{2}\left(\frac{t}{t_0} \right)^2 + 2i\pi f_0 t \right]$$

Strictly speaking the Morlet wavelet does not fully satisfy the conditions stated above because it is not a zero-mean function. However, in practice, when the product $2\pi t_0 f_0$ is in the range 5–6, the mean value of the wavelet is close to zero, and $g(t)$ contains a low number of oscillations (Nguyen et al., 1999). An estimation of the relative amplitude of each spectral component can be obtained by multiplying $\mathrm{CWT}_x^{(g)}(t,f)$ by $\sqrt{|f/f_0|}$. Furthermore, it is sometimes useful to calculate and plot the wavelet transform only for selected frequencies, for example those of the dominant spectral peaks.

2.4. Comparison between STFT and CWT

There is a strong similarity between the STFT and the CWT. Both time–frequency methods can be considered as the inner product of the signal $x(t)$ under consideration and a function $F(t,f)$. In the case of the STFT, this function is:

$$F(t,f) = g(t'-t)\cdot e^{-2i\pi ft'}$$

and in the case of the CWT, it is:

$$F(t,f) = \sqrt{|\frac{f}{f_0}|}\cdot g\left[\frac{f}{f_0}(t-t')\right]$$

There are two essential differences between the STFT and the CWT. The first difference is the distinct behavior of the time-shift/frequency-shift operators. Whereas the effective duration and bandwidth of the STFT are independent of the analysis frequency f, the effective duration of the CWT is inversely proportional to f, and the bandwidth is proportional to f (Kumar and Foufoula-Georgiou, 1997). The second difference is that the analyzing wavelet $g(t)$ is a low-pass signal in the STFT case, and a band-pass signal in the CWT case. Both of these techniques have the same time–frequency resolution limitations (time resolution and frequency resolution cannot be made arbitrarily good simultaneously). However, while the STFT resolution does not depend on the analysis frequency, the CWT has better time resolution and poorer frequency resolution at high frequency and better frequency resolution and poorer time resolution at low frequency.

2.5. Capon and Lagunas methods

The Capon (1972) method is a power level estimator, which consists in measuring the signal power by building a data-dependent band-pass filter (Lacoss, 1971). This filter must fulfil two conditions: (1) for a given frequency f_k, the frequency response is unity; and (2) the influence of the other spectral components of the signal is minimized. The solution to this problem of minimization under constraint is:

$$P_{\mathrm{Cap}}(f_k) = \frac{1}{S_k^{\mathrm{H}}\ R_x^{-1}\ S_k}$$

where R_x is the correlation matrix of the signal, $S_k{}^{\mathrm{T}} = [1,\ s_k,\ s_k{}^2,\ ...,\ s_k^p]$, $s_k = e^{2i\pi f_k \Delta t}$, p is the filter order, T and H denote respectively the transpose and the conjugate transpose, and Δt is the sampling interval.

The Lagunas (Lagunas-Hernandez and Gasull-Llampadas, 1984) method is derived from Capon's method and calculates the power spectral density of the signal by normalizing the power P_{Cap} by the bandwidth of the filter used in the power measure. The Lagunas spectral estimator is defined by:

$$D_{\mathrm{Lag}}(f_k) = \frac{S_k^{\mathrm{H}}\ R_x^{-1}\ S_k}{S_k^{\mathrm{H}}\ R_x^{-2}\ S_k}$$

Both methods can be applied on narrow sliding windows. This allows high-resolution estimations of the time–frequency distribution of the power, or power spectral density. There are no theoretical criteria for the choice of the filter order and window duration. Nevertheless, numerical experiments indicate that the order must be at least twice the number of peaks and must be increased for low signal to noise ratio. The number of samples in the window must be between three and five times the order (Fernandez and Martin, 1986; Adnet, 1990). The Lagunas estimator usually has a better frequency resolution, while Capon's estimator is more robust in the power estimations. It is thus convenient to use together both of these methods, which are well suited for the analysis of signals containing a few strong spectral components (Flandrin et al., 1992; Adnet, 1990).

2.6. Instantaneous frequency

Let us assume that near time t_0, the signal $x(t)$ can be approximated by $x(t) \approx A\ \cos[\Phi(t)]$, in which $\Phi(t) = 2\pi f_{\mathrm{i}}(t_0)t + \varphi_0(t_0)$ is the instantaneous phase, and $f_{\mathrm{i}}(t_0)$ and $\varphi_0(t_0)$ respectively are the instantaneous frequency and phase shift at time t_0. If $x(t)$ is a pure sinusoid $A\ \cos[2\pi f_0 t + \varphi_0]$, the instantaneous frequency f_{i} is constant and equals f_0. The frequency f_{i} is related to the derivative of Φ:

$$f_{\mathrm{i}}(t_0) = \frac{1}{2\pi}\left[\frac{\mathrm{d}\Phi(t)}{\mathrm{d}t}\right]_{t=t_0}$$

and $\Phi(t)$ is obtained by using the Hilbert transform $\mathrm{HT}[x(t)]$ of $x(t)$:

$$\Phi(t) = \tan^{-1}\left\{\frac{\mathrm{HT}[x(t)]}{x(t)}\right\}$$

The instantaneous frequency is easy to use and provides a good estimation of the dominant frequency of monotonic signals when the amplitude variations are not too rapid with respect to the period. Results are poor when the signal-to-noise ratio is low or when the signal includes several sinusoidal components. In that case the estimation can be greatly improved by band-pass filtering around the dominant frequencies (Brüstle, 1991).

2.7. Autoregressive modeling and deconvolution

The parametric methods consider a digital signal as the output y_n of a stationary linear filter excited by an input x_n. In the most general case, a new output sample depends on the preceding inputs and outputs:

$$y_n = \sum_{k=0}^{q} b_k x_{n-k} - \sum_{k=1}^{p} a_k y_{n-k}$$

The filter which relates the output to the input by the above linear difference equation can be characterized by the coefficients b_k and a_k, by its impulse response $h(t)$, or by the z-transform of $h(t)$:

$$H(z) = \frac{\sum_{k=0}^{q} b_k z^k}{1 + \sum_{k=1}^{p} a_k z^k} = K\frac{\prod_{k=1}^{q}(z - z_k)}{\prod_{k=1}^{p}(z - p_k)} = \frac{B(z)}{A(z)}$$

where z is a complex number, usually written as $z = \mathrm{e}^{-2i\pi f \Delta t}$ in geophysics (some authors use the alternative definition $z = \mathrm{e}^{+2i\pi f \Delta t}$), where Δt is the sampling interval, and f is the frequency. The z_k and p_k are, respectively, the zeroes and poles of the ARMA (autoregressive–moving average) filter $H(z)$. $B(z)$ and $A(z)$ represent, respectively, the MA and AR parts of $H(z)$.

Any causal and causally invertible filter, and thus minimum phase, can be represented either by an AR model of infinite order, or by an MA model of infinite order. Generally, it can also be approximated by an ARMA model of low order. The ARMA model is the easiest model to handle because only a limited number of coefficients are required to describe the process. A physical system that includes oscillators is minimum phase. Therefore, such a system can be modeled by an ARMA filter, the poles of which are related to the spectral peaks corresponding to the resonance frequencies. If the excitation of the oscillators, i.e., the filter input, has a white spectrum, the system is equivalent to a finite-order AR filter. This is the case when the excitation is composed of a single Dirac impulse, a large enough number of Dirac impulses with random spacings and amplitudes, or white noise. Otherwise a non-white spectrum excitation can be represented by a finite-order MA filter, and the entire system is equivalent to an ARMA filter of finite order. In practice, the coefficients a_k of the AR filter can be retrieved from the signal autocorrelation. If some additive white noise perturbs the signal, the presence of the noise modifies only the first few samples of the resulting autocorrelation, because the autocorrelation of white noise is a Dirac impulse. When estimating the AR coefficients, it is then possible to skip these samples which are related to the MA part of the filter. The corresponding relations are the modified Yule–Walker equations, which provide a rapid and robust estimation of the AR coefficients (see e.g., Marple, 1987, p. 181).

The simplest filter that can be associated to one spectral peak is an order-2 AR filter. In this case, the relation between outputs and inputs is:

$$a_0 y_n = x_n - a_1 y_{n-1} - a_2 y_{n-2}$$

and the z-transform of the impulse response is:

$$H^{\mathrm{AR2}}(z) = \frac{1}{a_0 + a_1 z + a_2 z^2} = \frac{1}{a_2 (z - p_0)(z - p_0^*)}$$

If the discriminant of the associated characteristic equation, $\Delta = a_1^2 - 4a_0 a_2$, is negative, this function has two complex conjugate poles p_0 and p_0^*. The AR2 filter is then equivalent to a harmonic oscillator governed by a second-order differential equation. There are simple correspondences between the poles p_0, coefficients a_k, and the reso-

nance frequency f_0 and quality factor Q of the oscillator (Bellanger, 1981). The poles are defined as:

$$p_0 = -\frac{a_1}{2a_2} + \frac{i}{2a_2}\sqrt{4a_0a_2 - a_1^2} = \rho\ \mathrm{e}^{-i\theta}$$

which yields the relations between the pole modulus and argument:

$$|p_0| = \rho = \left(\frac{a_0}{a_2}\right)^{1/2} \Rightarrow \frac{a_2}{a_0} = \frac{1}{\rho^2}$$

$$\mathrm{Re}(p_0) = \rho\cos\theta = -\frac{a_1}{2a_2} \Rightarrow \frac{a_1}{a_0} = -\frac{2\cos\theta}{\rho}$$

Furthermore, if the condition $\cos\theta < [(2\rho)/(1+\rho^2)]$ is satisfied, then the filter has a resonance frequency f_0 such as:

$$\cos(2\pi f_0 \Delta t) = -\frac{a_1\left(1 + \frac{a_2}{a_0}\right)}{4a_2} = \frac{\cos\theta}{2\rho}(\rho^2 + 1)$$

and a quality factor:

$$Q = \frac{\pi f_0 \Delta t}{1 - \frac{1}{\rho}}$$

When the poles are close to the unit circle (i.e., $\rho \approx 1$ and $Q \gg 2\pi f_0 \Delta t$), the filter displays a sharp resonance at the frequency f_0, and the following relations are obtained:

$$\cos(2\pi f_0 \Delta t) \approx \cos\theta \Rightarrow \theta \approx 2\pi f_0 \Delta t$$

In this case, the filter selects frequencies near f_0 and its impulse response is a decaying complex exponential. The AR2 filter is causal and minimum phase and its associated inverse filter is the order-2 MA filter with impulse response:

$$H^{\mathrm{MA2}}(z) = a_0 + a_1 z + a_2 z^2$$

Once the frequency f_0 and quality factor Q of a spectral peak are determined, it is easy to eliminate this peak by convolving the signal with the impulse response of the corresponding MA2 filter.

Most LP event and tremor spectra include a finite number of peaks indicating that either several oscillation modes of a resonator or various distinct resonators are excited. Each mode of each resonator corresponding to a spectral peak can be represented by one AR2 filter. Those filters are connected together either in series, in parallel, or in a combination of both. The shape of filter i is completely described by the ratios $a_1^i/{a_0}^i$ and ${a_2}^i/{a_0}^i$. The coefficients ${a_0}^i$ represent the amplification or attenuation factors, or the relative levels of excitation of the eigen-oscillations of a resonator.

In the serial case, the physical system is equivalent to M AR2 filters in a chain in which the input of filter 1 is the excitation function $e(t)$, and the output of filter M is the observed signal $x(t)$. Each filter is characterized by an impulse response, or its z-transform:

$$H_i(z) = \frac{1}{a_0^i + a_1^i z + a_2^i z^2}$$

The z-transform of the resulting impulse response of the entire system is the product of the M functions $H_i(z)$:

$$H^{\mathrm{S}}(z) = \prod_{i=1}^{M} H_i(z)$$

The corresponding inverse filter of the system is thus the product of the individual inverse filters:

$$\frac{1}{H^{\mathrm{S}}(z)} = \prod_{i=1}^{M} \frac{1}{H_i(z)} = \prod_{i=1}^{M} G_i(z)$$

with

$$G_i(z) = \frac{1}{H_i(z)} = a_0^i + a_1^i z + a_2^i z^2$$

Once the impulse response of each filter is estimated, it is easy to deconvolve the observed signal from the response of the whole system. The resulting time series is proportional to the excitation function $e(t)$, plus noise.

When the M filters are in parallel, the function $e(t)$ is the input to each filter and the resulting signal in the sum of all the filter outputs. The z-transform of the resulting impulse response is:

$$H^{\parallel}(z) = \sum_{i=1}^{M} H_i(z) = \sum_{i=1}^{M} \frac{1}{G_i(z)} = \frac{\sum_{i=1}^{M} \prod_{j\neq 1} G_j(z)}{\prod_{i=1}^{M} G_i(z)}$$

$$= H^{S}(z) \cdot \sum_{i=1}^{M} \prod_{j\neq i} G_j(z)$$

This is an ARMA filter, which has the same AR part $H^S(z)$ as the corresponding serial filter. It is thus easy to estimate the characteristics of the AR part and deconvolve the signal. Nevertheless, the MA part of the filter is not easy to calculate from the AR filter characteristics because the coefficients ${a_0}^i$, which determine the relative amplification of the various filters, are not given by the Yule–Walker algorithm. It is thus difficult to obtain the excitation function from the output of several parallel filters. The procedure, which consists in low-pass filtering the signal to isolate the fundamental mode and deconvolving the corresponding peak, does not always give results proportional to the excitation function. In this paper, only the AR part of the signals is deconvolved. More complex algorithms are required to process the MA part. It is easy to confirm the conclusions of this discussion by doing numerical experiments on synthetic signals.

When processing real signals, a further difficulty is to select the AR filter order. There is no general-use reliable criterion to determine the optimal order (Adnet, 1990). This order must be at least twice the number of peaks to be evaluated, but it is necessary to include some poles to take into account the noise and the eventual MA part of the filter. The estimated frequency and quality factor of the main spectral peaks must be stable with respect to the filter order. Furthermore, it may be useful to under-sample the signal in order to better spread the main poles over the Shannon frequency band.

The choice of the analyzed window of the signal is also important. At the onset of an LP event, for example, the influence of the excitation function $e(t)$ on the spectral content of the record can be strong, especially when it is not a Dirac impulse or white noise, and this can induce perturbations in the AR analysis when looking for the resonance frequencies. It is thus convenient to apply the AR modeling only on the event coda, i.e., after the excitation is over and when the signal is mainly composed of decaying sinusoids, but before the signal-to-noise ratio become too low. Furthermore, when using this approach, it is no more necessary to take into account a high-order MA filter to represent the non-white spectrum excitation. A time–frequency analysis of the record can help determine the window to analyze. In the case of tremor, the excitation is continuous. Such excitation may be considered as noise, so its influence on the signal spectrum and on the AR analysis is probably smaller. Furthermore, it is possible to carry out AR analysis on short-duration sliding windows of signal. In this case, only a small number of poles can be resolved, but this processing provides the temporal variations of the dominant frequencies with good resolution.

2.8. Spectral equalization

An alternative way to reduce the influence of harmonic components and enhance low-amplitude information is the use of spectral equalization, also named whitening techniques, which are frequently used for seismic prospecting data (Coppens and Mari, 1984). This method, which is very easy to implement, consists in reducing the differences between the amplitudes of the spectral peaks. This can be done, for example, by dividing the Fourier transform $S(f)$ of the signal by the square root of its power spectral density $P(f)$ plus a small constant to avoid divisions by zero. The Fourier transform of the resulting whitened signal is:

$$W(f) = \frac{S(f)}{\sqrt{\|P(f)\|} + \alpha \cdot \max(\sqrt{\|P(f)\|})}, \quad 0 \leq \alpha < 1$$

Furthermore, the whitening operator can be made causal by modifying the Fourier transform phase as (Oppenheim and Schafer, 1975, p. 346):

$$\varphi_{\min}(f) = \mathrm{HT}[\ln|W(f)|]$$

3. Examples of application

3.1. Synthetic signals

As a first example, we present an analysis of synthetic data. Two signals are obtained by convolving an excitation function $e(t)$ with the impulse response of a resonator $r(t)$, which includes two attenuated autoregressive processes (filter 1: $f_1 = 2$ Hz, $Q_1 = 30$, amplitude = 1; filter 2: $f_2 = 3.5$

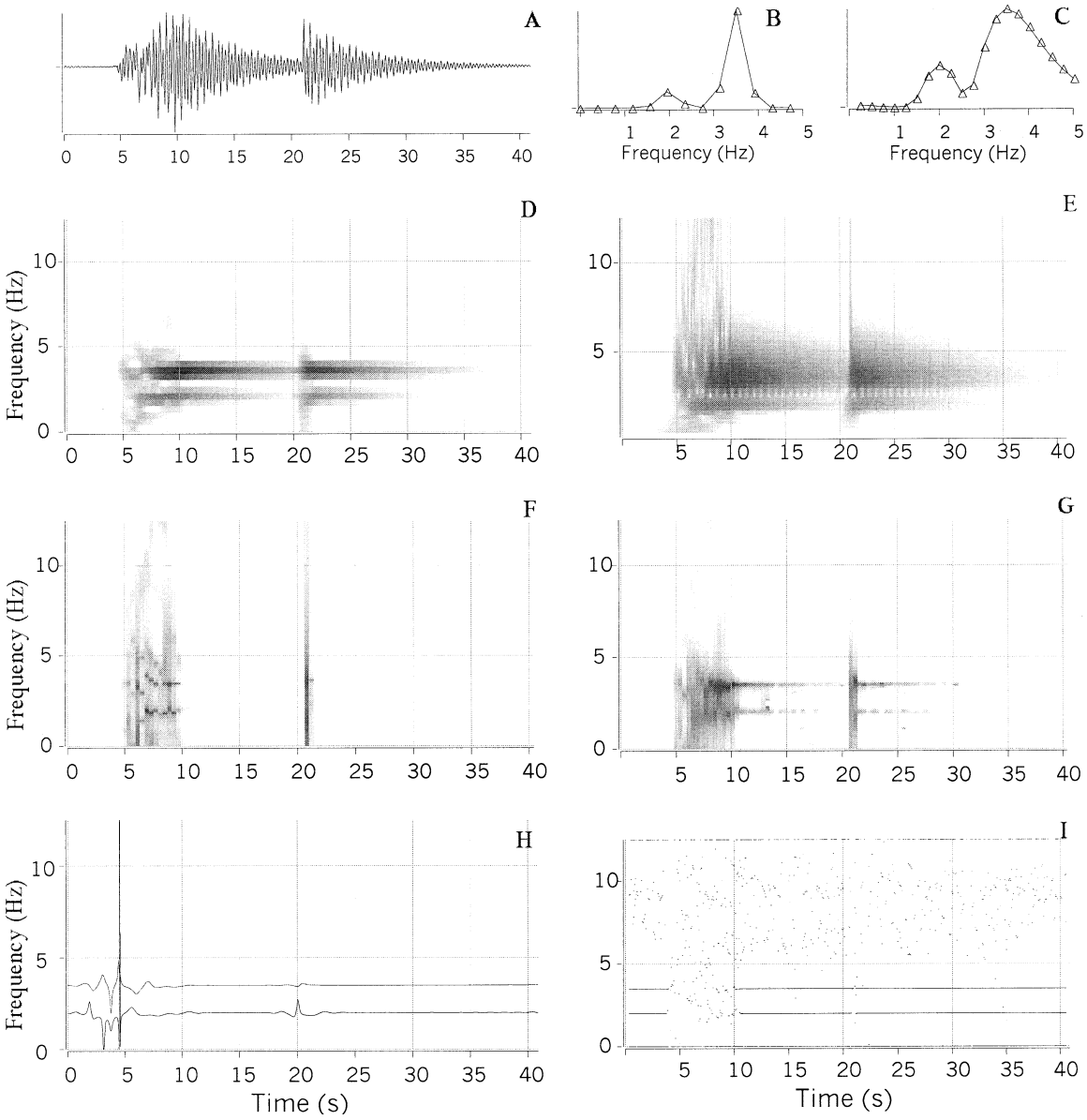

Fig. 1. Time–frequency analysis of a synthetic signal. The duration of the analysis windows is indicated in parentheses, when relevant. (A) Signal. (B) Cross-section in frequency of the STFT displayed in D at time $t = 24$ s. (C) Cross-section of the CWT displayed in E at time $t = 24$ s. (D) STFT (2.56 s). (E) CWT. (F) Capon's method (1.2 s). (G) Lagunas method (1.0 s). (H) Instantaneous frequencies in two 1-Hz-wide spectral bands centered at 2 and 3.5 Hz. (I) Autoregressive model on sliding window (0.8 s). A logarithmic amplitude scale has been used in D–G.

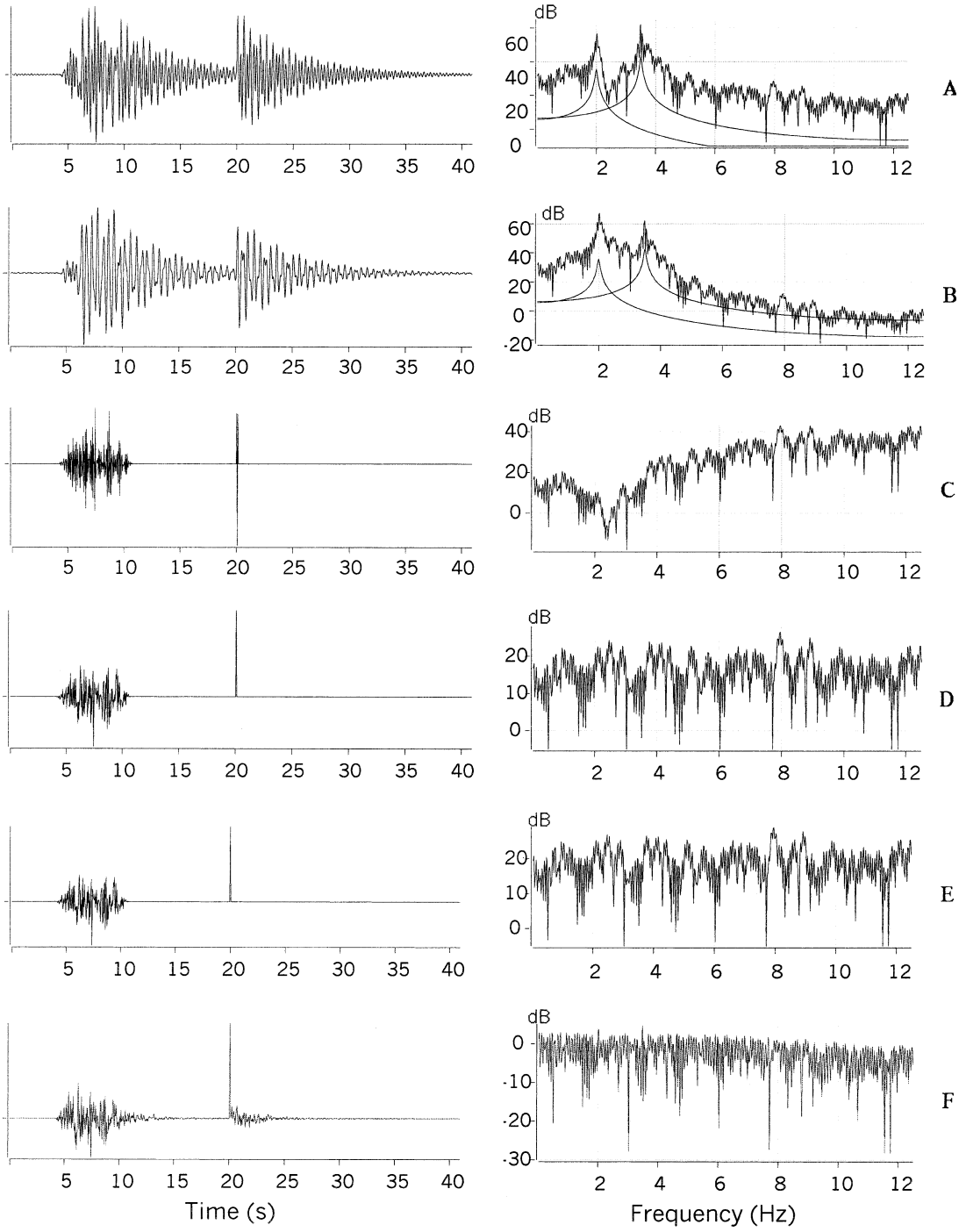
dB
A
B
C
D
E
F
5 10 15 20 25 30 35 40
2 4 6 8 10 12
Time (s)
Frequency (Hz)

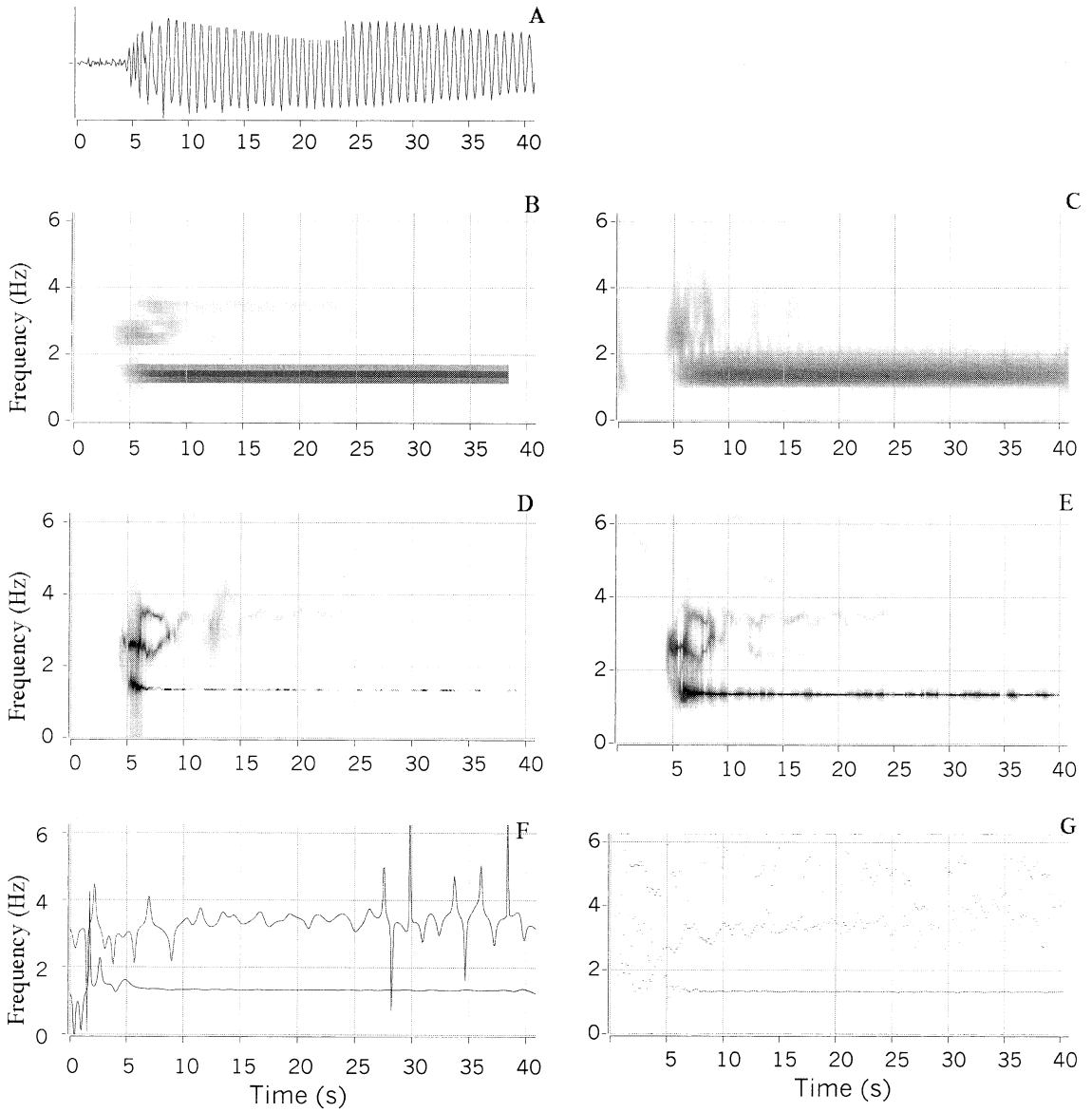

Fig. 3. Time–frequency analysis of an LP event at Galeras Volcano (Colombia). The duration of the analysis windows is indicated in parentheses, when relevant. (A) First 41 s of the record. (B) STFT (5.12 s). (C) CWT. (D) Capon's method (1.7 s). (E) Lagunas method (1.9 s). (F) Instantaneous frequency in spectral bands centered at 1.3 and 3.4 Hz. (G) Autoregressive modeling (1.4 s). Logarithmic amplitude scale for B–E.

Fig. 2. Deconvolution of two synthetic signals obtained by using two autoregressive processes connected either in parallel or in series. (A) Parallel-filters signal, and corresponding Fourier spectrum. (B) Serial-filters signal, and its spectrum. In A and B, the spectra of the impulse responses of both AR2 filters are also represented. (C) Parallel-filters signal after deconvolution, and its spectrum. (D) Serial-filters signal after deconvolution, and its spectrum. (E) Excitation function used for both synthetic data, and corresponding spectrum. The deconvolved signal is much more similar to the excitation function in the serial case than in the parallel one. (F) Causal spectral equalization of the serial filter signal, and corresponding spectrum; parameter α (see 2.8: Spectral equalization) is equal to 2×10^{-4}.

Hz, $Q_2 = 60$, amplitude = 2) connected either in parallel or in series. The common excitation function (Fig. 2E) is composed of two parts: (1) white noise tapered by a Hamming window (from 4 to 11 s); and (2) a Dirac pulse at $t = 21$ s. The resulting signals include 1024 values with a sampling frequency of 25 Hz. The time–frequency representations of the parallel-filters signal, obtained by the methods described above, are displayed in Fig. 1. As usual, the STFT (Fig. 1D) yields rough information in the frequency and time domains. The frequencies of oscillation are approximately determined but the power attenuation is well defined. While the Dirac pulse and white noise are well described in terms of energy in a large frequency band, their locations in time are not very precise. The analysis by CWT (Fig. 1E) produces approximately the same results as the STFT, except that the time–frequency plane has a different structure. Better resolution in time is achieved by using the CWT, especially for the Dirac pulse at $t = 21$ s which is well located at high frequency.

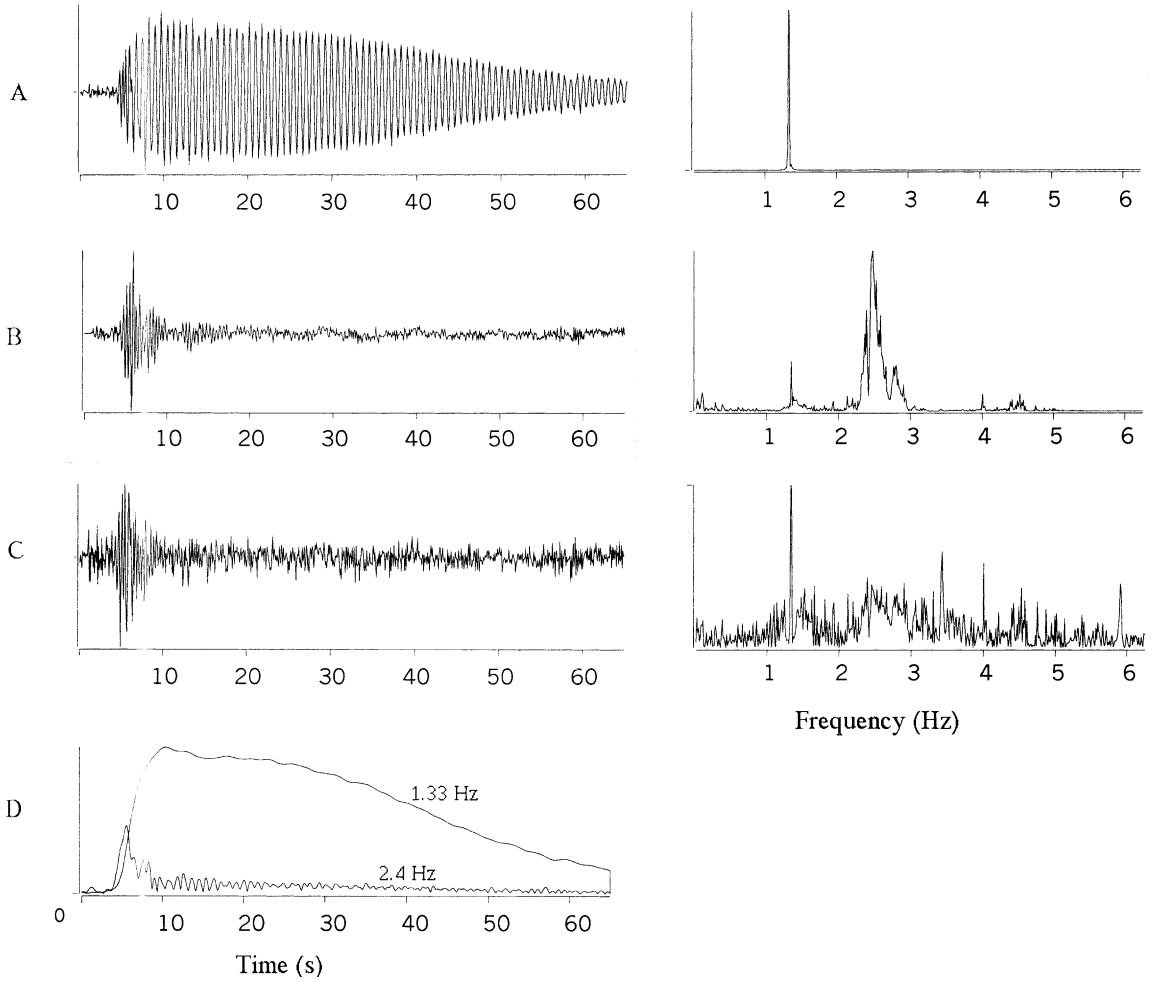

Fig. 4. LP event at Galeras. (A) First 65 s of the record, and corresponding spectrum. (B) Residual signal after deconvolving the dominant spectral component, and its spectrum. (C) Signal obtained by causal spectral equalization ($\alpha = 10^{-2}$), and corresponding spectrum. (D) Amplitude of the wavelet transform at the frequencies 1.33 and 2.4 Hz. All spectra are represented with linear amplitude scale. The main spectral peak at 1.335 Hz is well described by one AR2 filter and is almost completely eliminated by using the corresponding inverse MA2 filter. The amplitude of the wavelet transform at 2.4 Hz is similar to the envelope of the deconvolution residual.

The cross-section of the CWT at $t = 24$ s (Fig. 1C) illustrates that the frequency resolution increases when frequency decreases. Furthermore, at low frequency, CWT can provide more accurate values of the oscillation frequencies than STFT (Fig. 1B). Capon's method (Fig. 1F) yields information on power, and provides a good resolution of the two spectral peaks in the portion of the signal where their contributions are magnified by the excitation processes. In other parts of the signal, the spectral peaks vanish almost completely. The analysis by the Lagunas method (Fig. 1G) is characterized by high resolution in the time and frequency domains for the entire signal. Both the instantaneous frequency method and the autoregressive method (Fig. 1H,I) produce precise and robust estimations of the peak frequencies in the portions of the signal where the excitation is zero. Nevertheless, spectral information about the white noise and Dirac pulse is completely lost as these excitations cannot be represented by discrete frequencies. This example illustrates that a combination of several methods greatly improves the description of signals in the time–frequency plane.

Pure AR analysis of the parallel-filters signal yields an estimation of the frequency and quality factor of the decaying sinusoids:

$$f_1 = 2.00 \pm 0.02 \text{ Hz}, \; Q_1 = 30 \pm 7$$
$$f_2 = 3.50 \pm 0.02 \text{ Hz}, \; Q_2 = 60 \pm 10$$

where the errors are estimated from the dispersion obtained by varying the AR order. The first 15 s of the signal, which contain the excitation, are skipped for this analysis. Taking into account one MA coefficient in the Yule–Walker algorithm reduces the errors and leads to:

$$f_1 = 2.00 \pm 0.01 \text{ Hz}, \; Q_1 = 29.8 \pm 0.5$$
$$f_2 = 3.50 \pm 0.01 \text{ Hz}, \; Q_2 = 60.0 \pm 1.0$$

Both parallel-filters and serial-filters signals are then deconvolved by successively applying two MA2 filters corresponding to the two original AR2 filters used to construct the synthetic data. The resulting deconvolved signals, and their spectra, are compared with the original excitation in Fig. 2. As expected, in the serial case (Fig. 2B,D) the resulting signal is almost identical to the original excitation, while in the parallel case (Fig. 2A,C) the exact form of the excitation is not recovered. Furthermore, in the latter case, the MA part of the corresponding ARMA filter produces a zero in the residue spectrum. The spectral equalization (Fig. 2F) cancels the harmonic components of the signal and yields a good approximation of the excitation function.

Table 1
Frequencies and quality factors estimated by the AR analysis of the coda of several events

Signal spectral band	Frequency (Hz)	Error (Hz)	Quality factor	Error
Galeras LP event [0–6.25 Hz]	1.335	0.005	170	30
	3.40	0.04	30	5
	5.85	0.05	20	6
Purace LP event [0–12.5 Hz]	4.93	0.01	150	40
	8.21	0.01	260	60
	10.02	0.01	230	40
	10.86	0.01	280	50
Misti LP event [0–12.5 Hz]	2.53	0.03	23	8
	4.39	0.01	210	60
	7.21	0.03	80	50
	9.16	0.03	200	100
	12.26	0.03	90	40
Ruapehu tremor [0–6.25 Hz]	2.08	0.06	11	4
	2.94	0.06	10	3
	6.20	0.04	25	7

Errors are estimated from the parameter variability obtained by changing the total AR order.

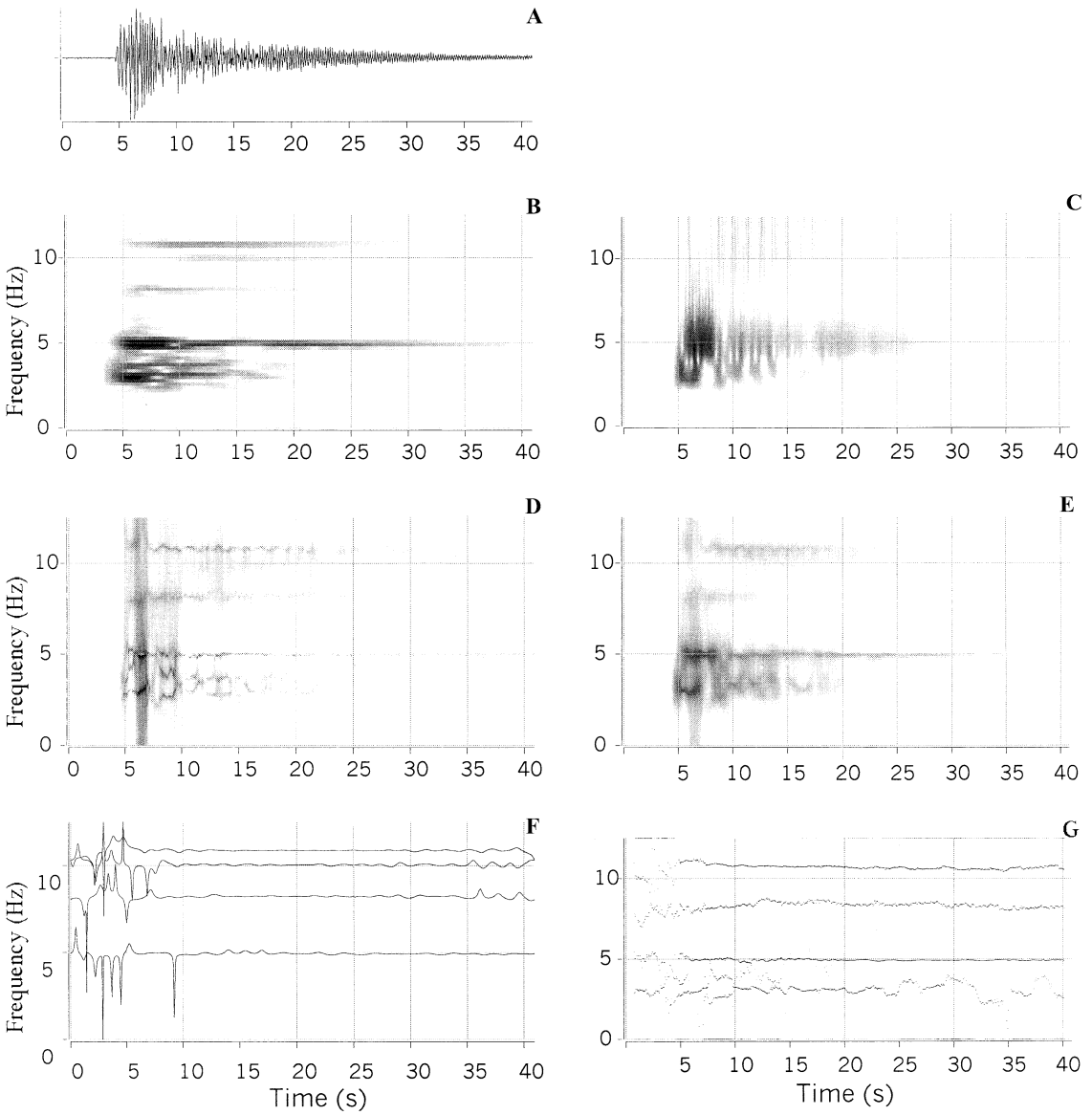

Fig. 5. Time–frequency analysis of an LP event at Purace Volcano (Colombia). (A) Seismogram. (B) STFT (5.1 s). (C) CWT. (D) Capon's method (1.2 s). (E) Lagunas method (1.4 s). (F) Instantaneous frequencies in spectral bands centered at 4.9, 8.2, 10.0, and 10.8 Hz. (G) AR modeling (1.6 s). Logarithmic amplitude scale for B–E.

3.2. LP event at Galeras Volcano

Figs. 3A and 4A show an LP event recorded at Galeras Volcano, Colombia on June 5, 1993 (Gómez and Torres, 1997). The record is from station CRA (1 Hz vertical seismometer) of the Galeras network. This signal contains a dominant spectral peak at 1.33 Hz (Fig. 4A), and small secondary peaks at 3.4 and 5.9 Hz which are not visible on a graph with a linear scale. The time–frequency diagrams obtained by several methods (Fig. 3B–G) indicate that the frequency of the main peak is constant along the entire signal, and that the corresponding energy arrives about 1 s after

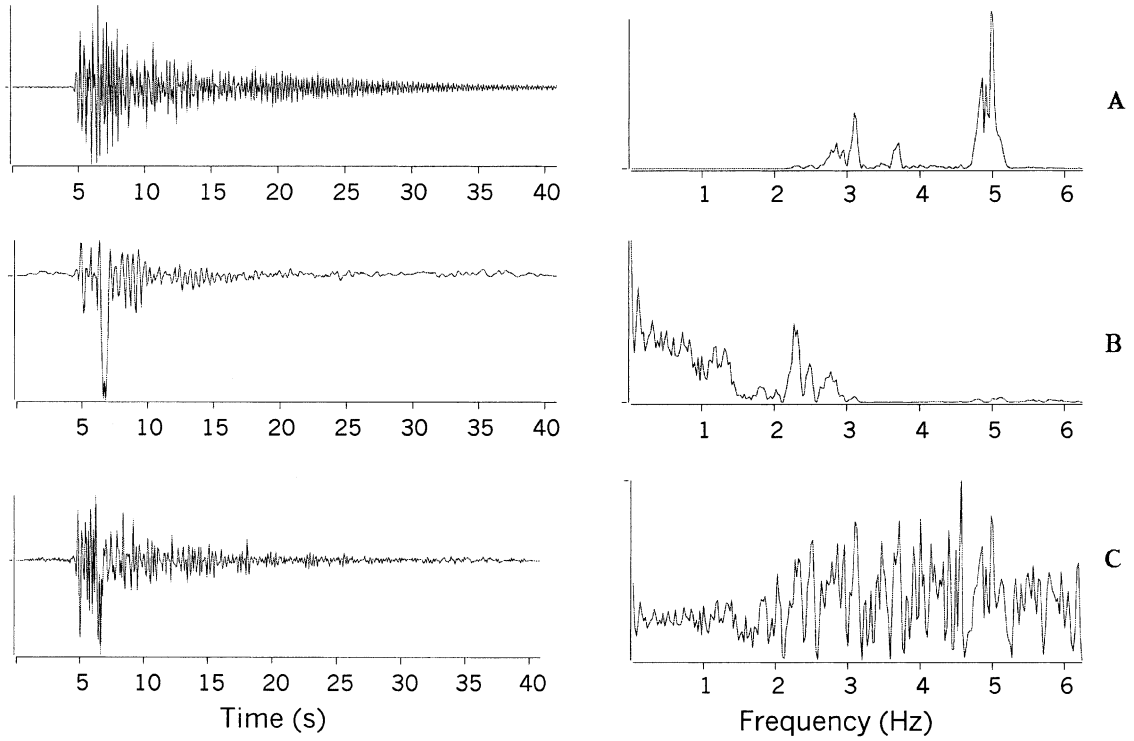

Fig. 6. LP event at Purace. (A) Record, and its spectrum. (B) Residual signal after deconvolving the dominant spectral components, and corresponding spectrum. (C) Signal obtained by causal spectral equalization ($\alpha = 10^{-2}$), and its spectrum. A large negative pulse is obtained by both deconvolution and spectral equalization.

the first arrival. It also reveals a seismic phase near the seismogram onset, with frequency of about 2.4 Hz and duration of roughly 4 s (Fig. 3B–E).

A more precise AR analysis is then carried out by using the Yule–Walker algorithm. The first 25 s of the signal, which contain the excitation, are deleted and a 40.96-s-long duration is used. This makes it possible to resolve several poles in the seismogram coda (Table 1). The main spectral peak is characterized by $f = 1.335 \pm 0.005$ Hz and $Q = 170 \pm 30$. Fig. 4B shows the residual signal and its spectrum after deconvolving the dominant spectral components (1.33, 3.4, and 5.9 Hz). It includes a short-duration oscillation of about 5 s in the band [2.3–2.8 Hz] which is also detected by the time–frequency analysis. After this oscillation, the residual signal amplitude decreases until $t \approx 20$ s and then remains constant. The signal obtained by spectral equalization (Fig. 4C) shows similar features. However, the corresponding spectrum is whiter and does not display as clearly the spectral content of the excitation. The amplitudes of the wavelet transform at frequencies 1.33 Hz and 2.4 Hz are displayed in Fig. 4D. It shows the short-duration phase at the beginning of the record. The amplitude at 1.33 Hz is similar to the signal envelope. It reaches its maximum 5.5 s after the first arrival, slowly decreases during 15–25 s and then decreases faster. The results obtained by the different analysis methods suggest that the source resonator is first strongly excited during 4–5 s at the beginning of the event. Next, the resonance is sustained by a low-level excitation during about 20 s in the same manner as a volcanic tremor. The coda, which corresponds to the free oscillation of the resonator, actually begins after this period of low-level excitation.

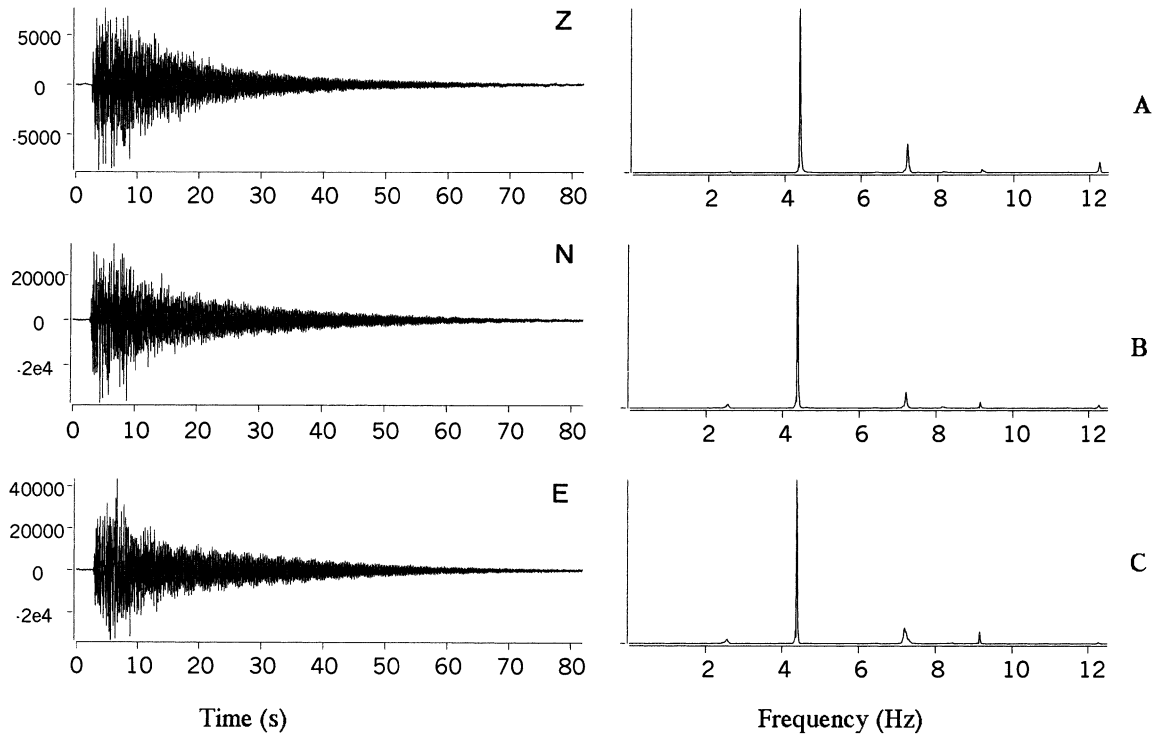

Fig. 7. LP event at Misti Volcano (Peru). Records of the three components and their Fourier spectra. (A) Vertical component. (B) North component. (C) East component.

3.3. LP event at Purace Volcano

This LP event (Figs. 5A and 6A) was recorded at station CUR, located about 1 km from the crater of Purace Volcano, Colombia, on September 15, 1994 (Gómez and Torres, 1997). It is characterized by several spectral peaks, the frequencies of which are almost constant during the entire signal (Fig. 5B–G). The time–frequency analysis reveals that the main spectral component ($f = 4.93$ Hz) is preceded by an arrival at lower frequency (~ 3 Hz). This feature is particularly well resolved by the CWT and the Lagunas method (Fig. 5C,E). The AR modeling of a 40.96-s-long window in the coda (after deleting 10 s at the record onset) requires a relatively high-order AR filter with a small MA part. The frequency and quality factor of the main poles are given in Table 1. The residual signal obtained by applying the corresponding inverse filters (Fig. 6B) includes a large negative pulse about 1.7 s after the first arrival. The causal spectral equalization applied to the same record produces similar results (Fig. 6C), although, as expected, the corresponding spectrum is much whiter.

3.4. LP event at Misti Volcano

This LP event, displayed in Fig. 7, was recorded on April 7, 1998, by a three-component short-period temporary station located close to the crater of Misti Volcano, Peru (Métaxian, personal communication). The corresponding Fourier spectra (Fig. 7) contain a main peak at 4.4 Hz and several secondary peaks (2.5, 7.2 Hz, 9.2 Hz, 12.2 Hz, etc.). Fig. 8 shows results of the time–frequency analysis of the vertical component performed by several methods. Similar diagrams are obtained for the horizontal components. The STFT (Fig. 8B) has a poor time resolution and reasonable frequency resolution, which makes it possible to see up to six spectral components

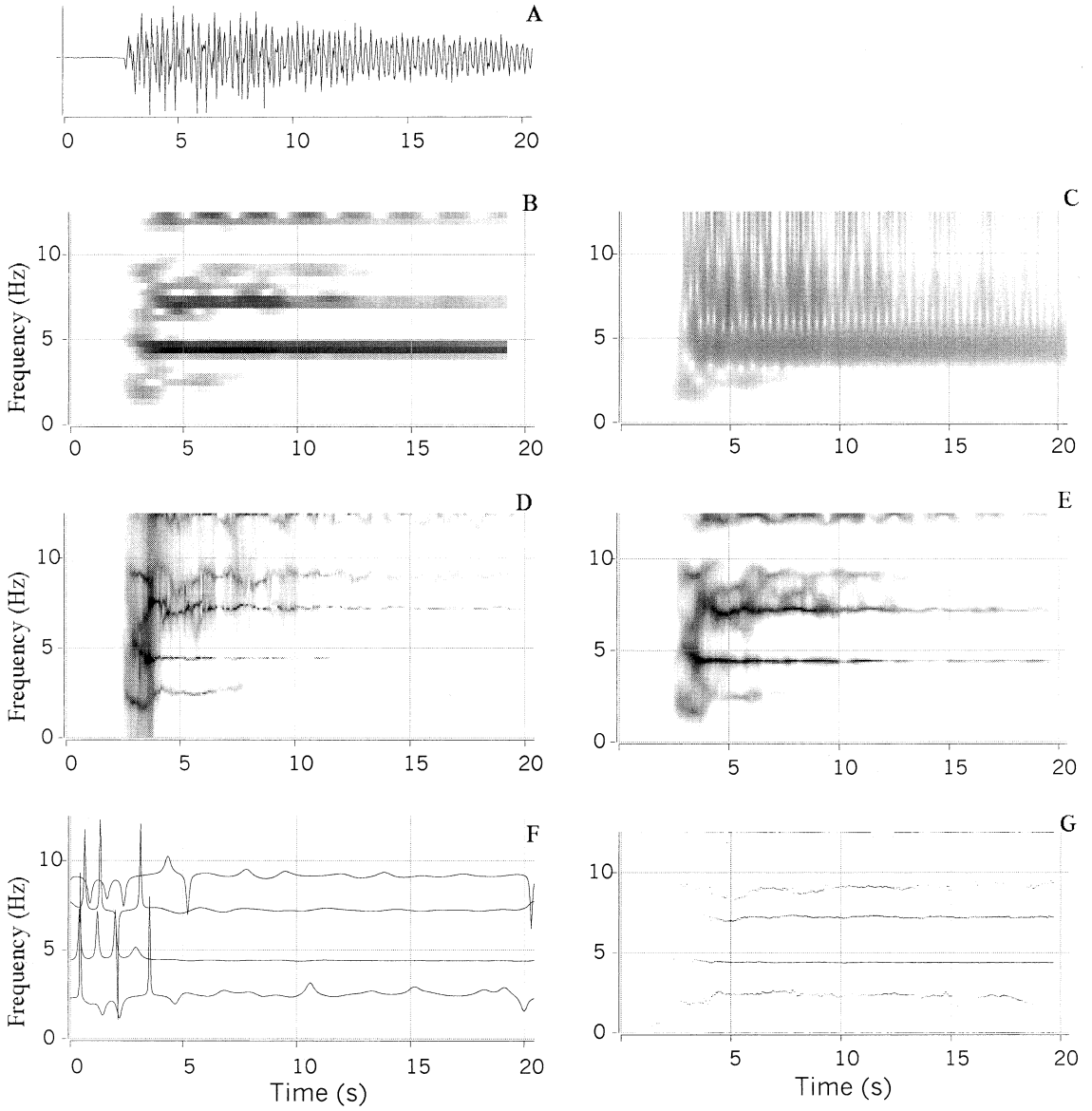

Fig. 8. Time–frequency analysis of the vertical component of the LP event at Misti. (A) First 20.5 s of record. (B) STFT (2.56 s). (C) CWT. (D) Capon's method (0.6 s). (E) Lagunas method (0.8 s). (F) Instantaneous frequencies in spectral bands centered at 2.5, 4.4, 7.2, and 9.2 Hz. (G) AR modeling (0.8 s).

along the signal. The low-frequency resolution of the CWT (Fig. 8C) prevents the identification of high-frequency spectral peaks – notice, for example, the spreading of the 7.2-Hz peak. On the other hand, both the STFT and CWT show an arrival of short duration (<2 s) and low frequency (<2 Hz) at the beginning of the event. The Capon and Lagunas methods (Fig. 8D,E) clearly have better time and frequency resolutions and can resolve four spectral peaks (4.4, 7.2, 9.2, and 12.2 Hz). The instantaneous frequency in four spectral bands has been calculated by successively applying 1-Hz-wide band-pass filters centered at the frequencies of four peaks (Fig.

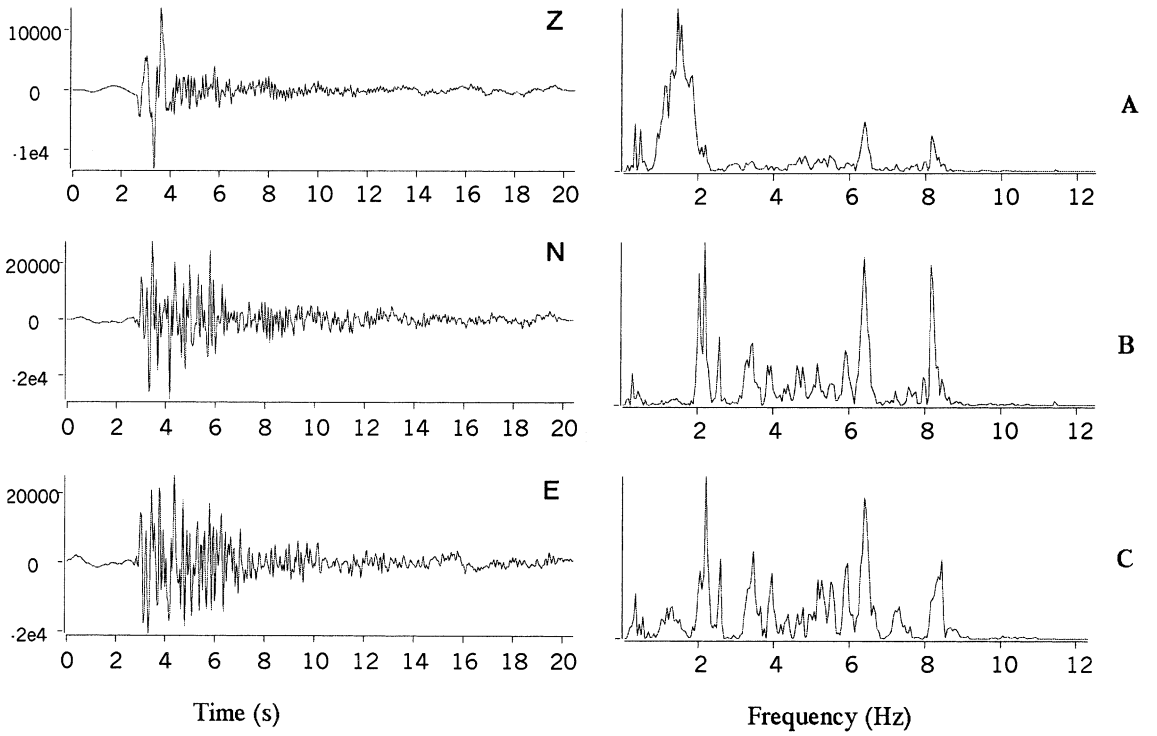

Fig. 9. First 20 s of the residual signals obtained by deconvolving the main spectral components of the three-components of the Misti event and their Fourier spectra. (A) Vertical component. (B) North component. (C) East component.

8F). The AR analysis, with a 0.8-s-long sliding window, yields similar results for the time variation of the main spectral peaks frequencies (Fig. 8G).

By compiling and comparing the results from the different time–frequency methods, it is possible to extract several robust features from the records. (1) Several dominant spectral components are present during almost the entire signal duration and their frequencies are constant in the coda. (2) The energy corresponding to the main spectral peak (4.4 Hz) seems to arrive 0.5–0.8 s after the first arrival. (3) The frequency of the main peak slightly decreases, from about 5 Hz to 4.4 Hz, during the first 0.5–0.7 s. In the event coda, the frequency of the main peak is very stable. (4) At the very beginning of the vertical seismogram, a low-frequency (<2 Hz) phase of short duration is detected by all the methods. This arrival is not present in the horizontal components.

For a precise AR analysis with the Yule–Walker algorithm, the first 20 s of signal are deleted and 40.96-s-long signal windows are used. Table 1 lists the estimated frequency and quality factor for the five principal poles. The main spectral peak is characterized by a frequency $f = 4.39 \pm 0.01$ Hz and quality factor $Q = 210 \pm 60$. Similar results are obtained for all three components. In contrast, the Q factors of the secondary poles sometimes differ significantly between different components.

Next, the effects of the dominant spectral peaks are eliminated by filtering the signal with a series of MA2 filters. Fig. 9 displays the resulting deconvolved signals, and their spectra, for the three components. An interesting feature of these residues is the presence of a short-duration (~ 1.7 s) low-frequency arrival at the onset of the vertical component. This phase was already revealed by the time–frequency analysis and is not observed in the residues of the horizontal components.

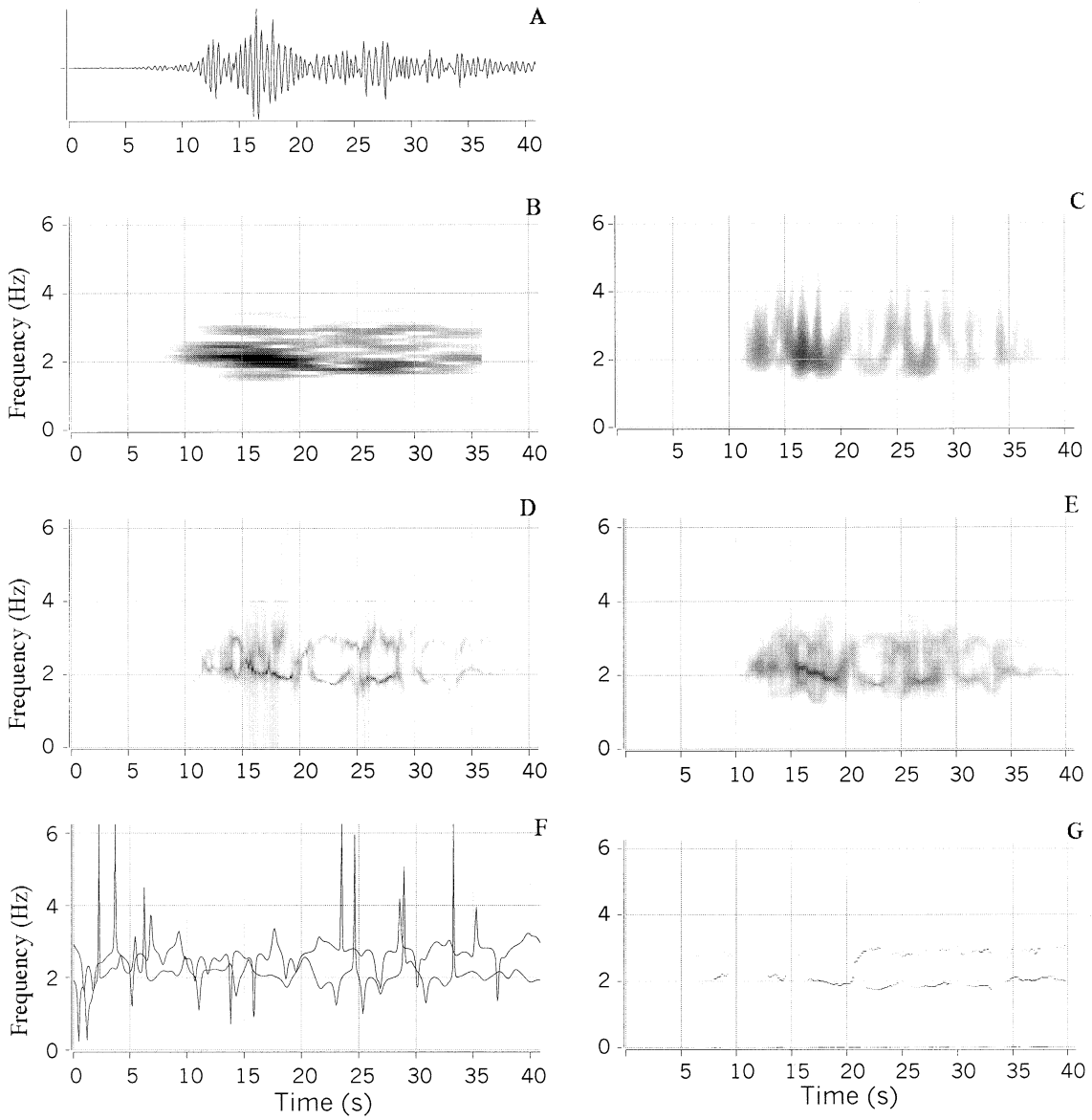

Fig. 10. Time–frequency analysis of volcanic tremor at Ruapehu Volcano (New Zealand). (A) Record. (B) STFT (5.12 s). (C) CWT. (D) Capon's method (1.6 s). (E) Lagunas method (2.4 s). (F) Instantaneous frequencies in spectral bands centered at 2.0 and 2.9 Hz. (G) AR modeling (2.4 s).

After their onset, the amplitude of the residual signals progressively decreases during more than 10 s.

3.5. Tremor at Ruapehu Volcano

The next example (Figs. 10A and 11A) shows the onset of volcanic tremor at Ruapehu Volcano, New Zealand, recorded at station DRZ on August 5, 1990 (Hurst, personal communication). The Fourier spectrum (Fig. 11A) shows that most of the energy is in the band [1.5–3.0 Hz]. The time–frequency representations of this signal have a complex structure. The highest-resolution

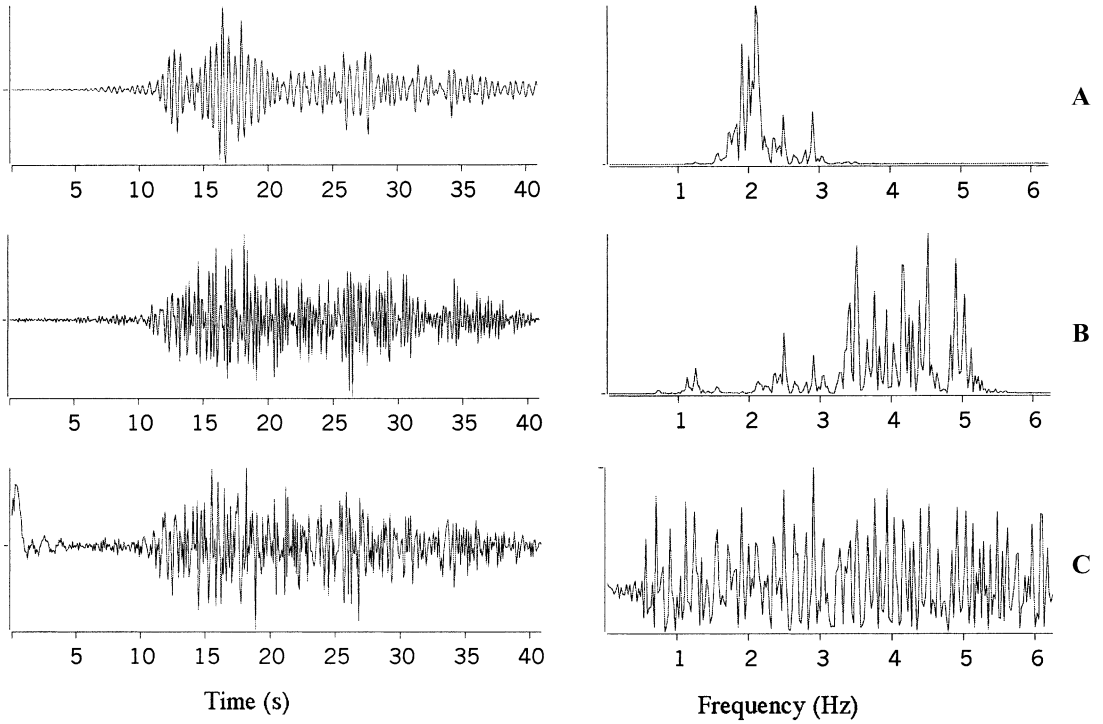

Fig. 11. Volcanic tremor at Ruapehu. (A) Original signal and its spectrum. (B) Residual signal after deconvolving the dominant spectral components, and corresponding spectrum. (C) Signal obtained by spectral equalization ($\alpha = 10^{-3}$), and its spectrum.

analysis (Fig. 10D–G) points to rapid fluctuations of the frequency of the dominant spectral components. Similar fluctuations are also observed in other records of Ruapehu tremor. The CWT (Fig. 10C) displays many short-duration, broadband peaks, which coincide with a series of energy bursts. AR modeling of the whole signal identifies a main pole with frequency $f = 2.08 \pm 0.06$ Hz ($Q = 11 \pm 4$) and secondary poles at 2.94 and 6.20 Hz (Table 1). A more detailed analysis of the first 10 s of the record shows that oscillations at a frequency of about 2.1 Hz are also present in the noise before the tremor. After deconvolution or spectral equalization, the residual signal (Fig. 11B,C) is characterized by a broadband spectrum and by an amplitude which varies rapidly and simultaneously with the tremor amplitude. In the present case, estimations of the quality factor probably do not provide an accurate picture of the resonator properties because the analyzed signal includes a non-stationary excitation process.

3.6. LP events at Kelut Volcano

As a final example, we present the analysis of a set of 16 LP events (Fig. 12A and Table 2) which were recorded from December 25, 1989 to January 7, 1990, i.e., about a month before the February 10, 1990 eruption of Kelut Volcano, Java (Lesage and Surono, 1995). The station features a 1-Hz vertical seismometer and is located inside a tunnel about 500 m from the crater. All the events have short durations and low amplitudes and their spectra (Fig. 12B) are characterized by one dominant peak in the range [5.0–6.2 Hz]. There are some double events.

Fig. 13 displays the results of time–frequency analysis performed on one of the events. These clearly show high-frequency arrivals at the onset of the seismogram and during the second part of the double event. The dominant frequency is constant over the entire signal. Estimations of the frequency and quality factor of the main spectral peak, obtained using the Yule–Walker algorithm,

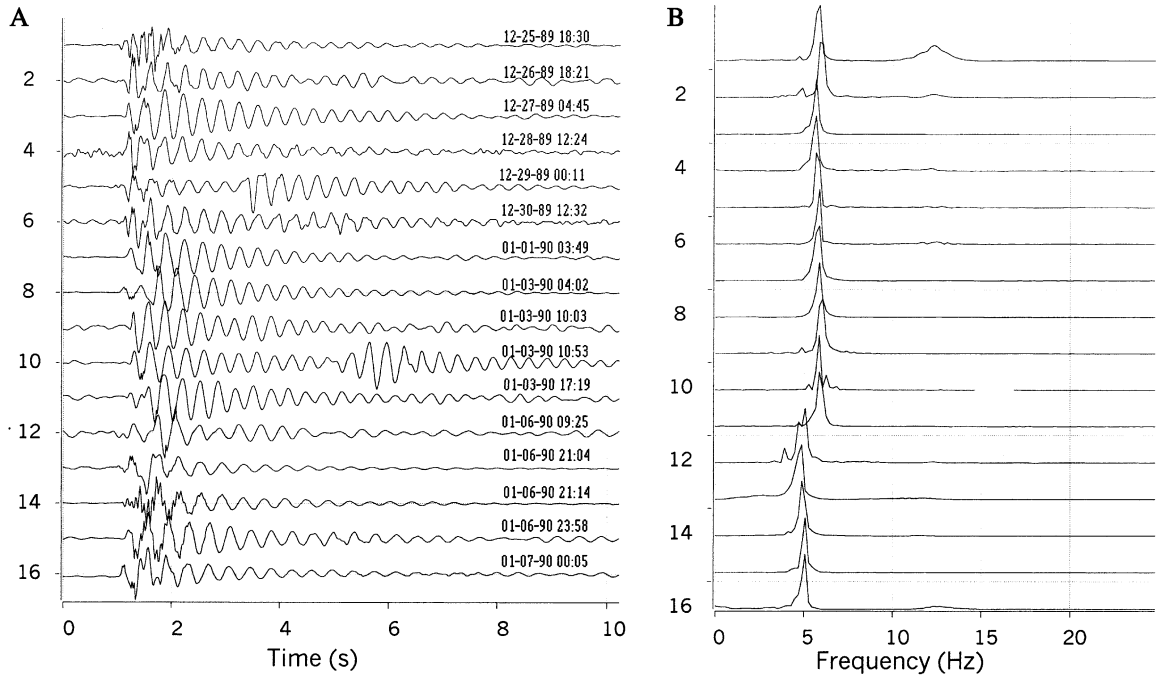

Fig. 12. (A) LP events at Kelut Volcano (Java). (B) Their Fourier spectra.

are given in Table 2. Filters including a small number of complex poles (6–12) allow an accurate modeling of the resonance effects. In some cases, the introduction of an MA1 filter in the algorithm improves the result. Table 2 indicates that the main frequency is generally stable between events within intervals ranging from one to a few days. From December 25, 1989 to January 1, 1990, the frequency equals 5.9 ± 0.05 Hz, besides one event with $f = 6.23$ Hz. On January 3, its value is about 6.15 Hz and during days 6 and 7, it is in the range 5.04–5.40 Hz. The values of Q are in the interval 13–30, but this greater variability is probably due in part to estimation errors.

Fig. 14 displays the residual signals, obtained by deconvolving the main spectral peak, and the corresponding Fourier spectra. The resulting excitation functions are very short. Their durations are between 0.2 and 0.9 s, although most durations are near 0.7 s. For six events, the excitation is divided into two parts, the first of which is generally more impulsive with a higher frequency content. The second part arrives between 0.3 and 1.8 s after the first arrival and consists of either another short pulse or a progressive increase of the amplitude. The polarity of the first arrival of the excitation functions is generally positive although some of them are negative or emergent. A large part of the excitation function energy is concentrated in a narrow band – a few Hz wide – centered between 12 and 16 Hz. The residual signals also include higher-frequency energy, which could be noise.

4. Discussion

In this paper, we have presented a small selection of signal processing methods among the great variety of methods that are available today. Our main objective was to emphasize, through a few examples, the abilities – and limitations – of these methods to produce interesting information about the physical processes related to LP events and volcanic tremor.

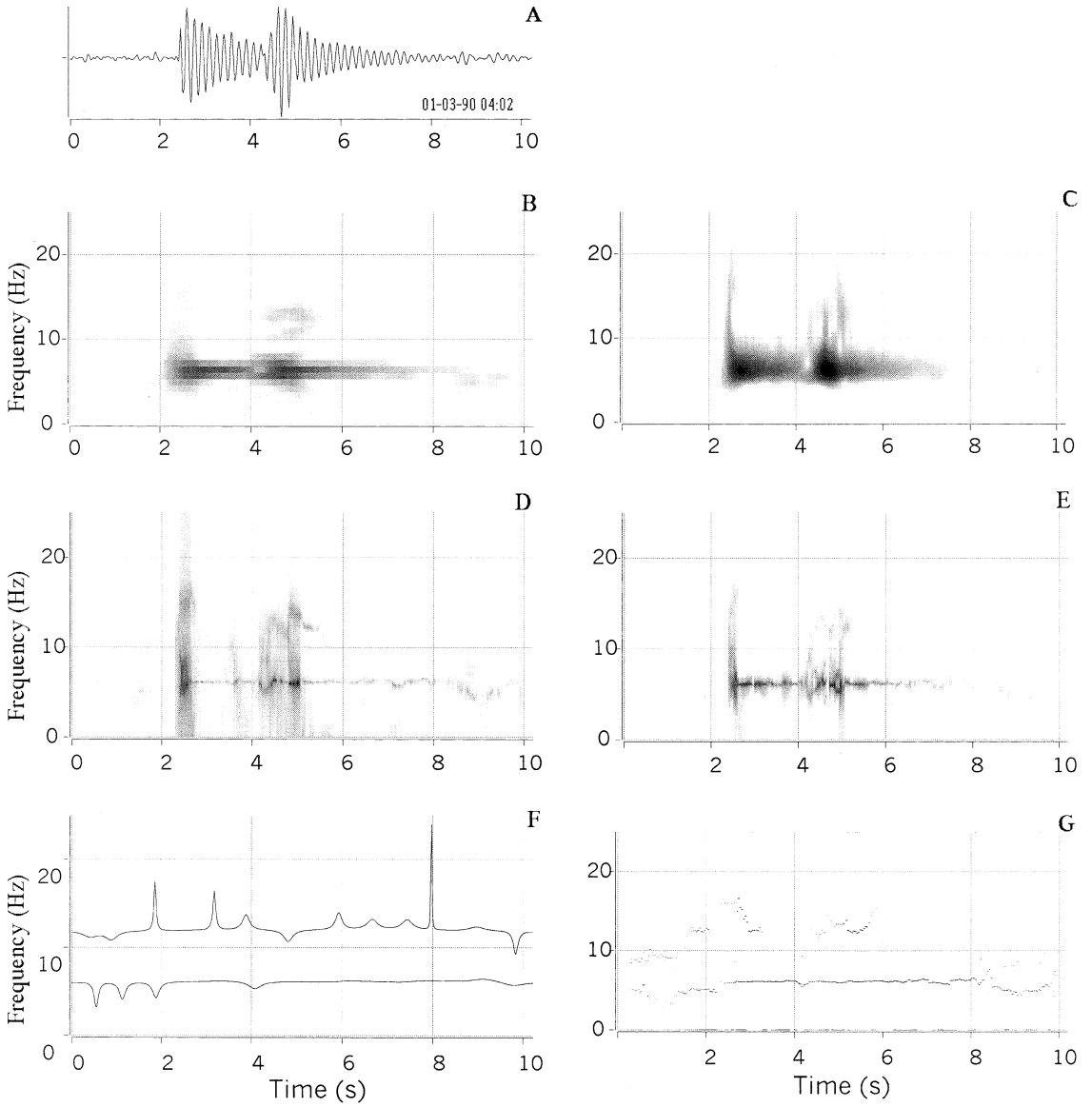

Fig. 13. Time–frequency analysis of Kelut LP event at 04:02 h on January 3, 1990. (A) Signal. (B) STFT (1.28 s). (C) CWT. (D) Capon's method (0.4 s). (E) Lagunas method (0.4 s). (F) Instantaneous frequencies in bands centered at 6 Hz and 12 Hz. (G) AR modeling (0.6 s). The CWT, Capon and Lagunas methods all clearly display the broadband and short-duration characteristics of the first arrival.

4.1. Time–frequency analysis

The STFT yields the rough features of a signal in the time–frequency domain. Although it has limited resolution, it is widely used because of its robustness and the ease with which it can be programmed from fast Fourier transform subroutines. The CWT resolution is not constant in the time–frequency domain. This property makes it possible to detect some details which are not revealed by the STFT method. For example, the time resolution of an impulsive arrival is much better at high frequency in the CWT. The Capon and Lagunas methods can produce high-resolu-

Table 2
Same as Table 1 for the 16 LP events of Kelut Volcano

No.	Date and hour	Frequency (Hz)	Error (Hz)	Quality factor	Error
1	89/12/25 18:30	5.89	0.05	20	2
2	89/12/26 18:21	6.23	0.02	30	10
3	89/12/27 04:45	5.86	0.04	22	4
4	89/12/28 12:24	5.85	0.02	30	10
5	89/12/29 00:11	5.91	0.02	25	3
6	89/12/30 12:32	5.91	0.04	20	4
7	90/01/01 03:49	5.91	0.04	17	3
8	90/01/03 04:02	6.08	0.03	13	2
9	90/01/03 10:03	6.22	0.02	23	3
10	90/01/03 10:53	6.22	0.04	25	7
11	90/01/03 17:19	6.23	0.03	24	5
12	90/01/06 09:25	5.40	0.06	18	4
13	90/01/06 21:04	5.04	0.02	24	4
14	90/01/06 21:14	5.08	0.02	24	4
15	90/01/06 23:58	5.15	0.05	13	2
16	90/01/07 00:05	5.15	0.08	16	4

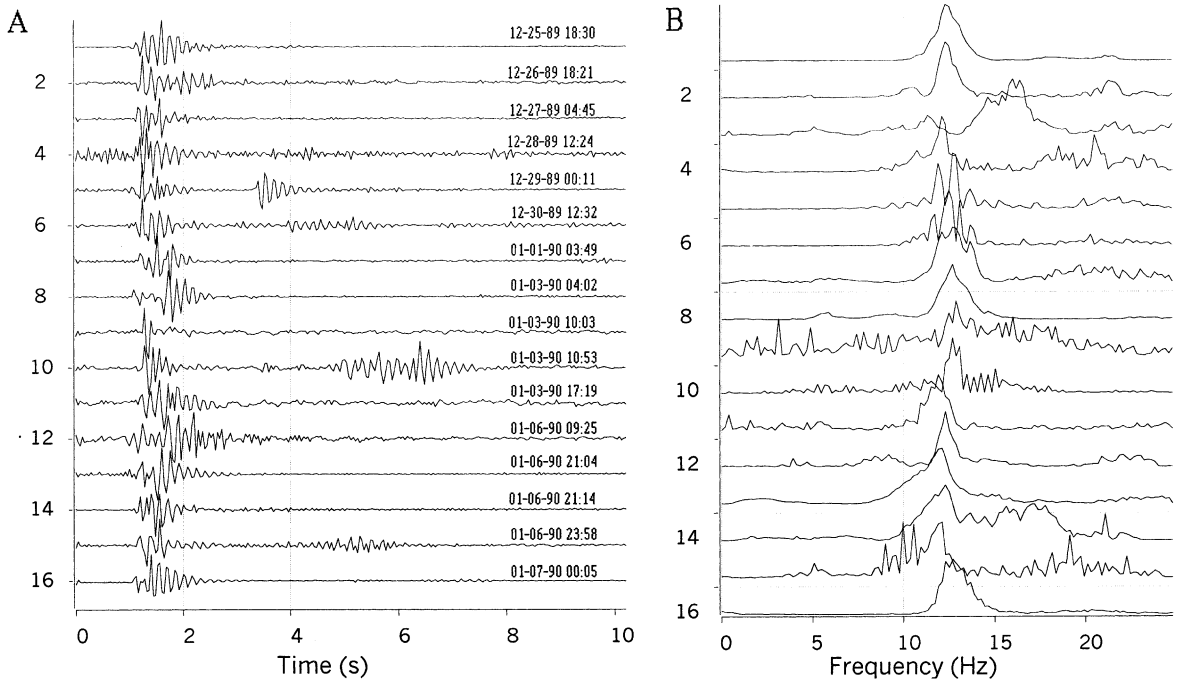

Fig. 14. (A) Residual signals obtained by deconvolving the main spectral component of the Kelut LP events. (B) Corresponding Fourier spectra.

tion time–frequency representations, especially for signals that contain strong harmonic components such as LP events and volcanic tremor. Nevertheless, the results are somewhat dependent on window length and filter order. The sliding AR analysis yields precise estimations of the spectral peak frequencies with good time resolution. Although it does not produce a complete description of the time–frequency space, it can be used to measure rapid frequency gliding of volcanic tremor. The instantaneous frequency yields roughly similar information, but it is very sensitive to noise and requires a priori band-pass filtering around each spectral peak frequency. The analysis of the synthetic and real signals presented above illustrates that the simultaneous use of several time–frequency methods greatly improves the description of the recorded phenomena.

4.2. Autoregressive analysis and deconvolution

The autoregressive modeling and related deconvolution of the records offer interesting perspectives for the analysis of signals that include resonator effects. While the dominant spectral peaks provide information on the acoustic properties of the source resonator, it can preclude the observation of other phenomena involved in the generation of the event. The removal of the principal decaying sinusoids that are included in the records, via the use of data-dependent filters, produces residual signals which contain, in some form, the excitation function of the resonators. Nevertheless, this kind of method cannot separate the excitation and the propagation and site effects. Such a separation would require the knowledge of Green's functions and site response.

The main spectral peak of a monochromatic event may be modeled by one AR2 filter. In this case, the deconvolved signal yields a direct estimation of the excitation function if the noise level is low enough. On the other hand, when dealing with more complex signals, it is difficult to determine whether the system can be represented by serial or parallel filters, or by a complex combination of both. In the serial case, a first resonator is excited and radiates waves which excite a second resonator and so on. A single mode of fluid-filled cavity embedded in a structure that includes a shallow soft layer inducing a resonance effect is an example of serial filters. In the more common non-serial cases, the residual signal obtained by AR analysis and deconvolution does not provide directly the waveform of the excitation function, because it is not possible to deconvolve the MA part of the corresponding filter with the methods presented here. In any case, the residual contains information, including duration, arrival time and some spectral characteristics of the excitation, which can help constrain the physical source models. The spectral equalization easily yields rough information on the non-harmonic part of the signal. It can be used, for example, to estimate the duration of the excitation process.

The AR analysis yields precise estimations of the resonance frequencies as long as (1) the results are stable with respect to the AR order, and (2) the analyzed signal window does not include the excitation function. However, when the excitation can be described by one Dirac impulse or by continuous noise with wide band spectrum, as in the case of tremor, the calculated frequency is not significantly affected by the excitation. On the other hand, the quality factors of the resonators are estimated with higher precision in the coda when the excitation is no longer active and the analyzed signal is mainly composed of decaying sinusoids. However, numerical experiments show that the results of the deconvolution are not very sensitive to errors on the Q values.

4.3. Application to seismovolcanic signals

Among the examples presented above, the main resonance peaks of three LP events are characterized by high values of the quality factor (Galeras: $f=1.33$ Hz, $Q=160$; Purace: $f=4.92$ Hz, $Q=180$; Misti: $f=4.4$ Hz, $Q=200$). Kumagai and Chouet (1999) give a consistent estimation of Q for LP event at Galeras. On the basis of the acoustic properties of various mixtures of liquid, gas and ash, and carrying out numerical simulations of the radiation of a fluid-driven crack, Kumagai and Chouet (1999, 2000) conclude that Q values in the range 160–200 can be generated by a resonator filled with a basalt–gas mixture or

with dusty or misty gas. In contrast, the quality factors are very low for the 16 LP events of Kelut (20 on average) and for the Ruapehu tremor (10–25). These values are consistent with a crack filled with either water or basalt including a small gas volume fraction (Kumagai and Chouet, 1999, 2000). Nevertheless, the existence of crater lakes with degassing inside at both volcanoes and their andesitic nature suggest that the resonator is probably filled with bubbly water (Lesage and Surono, 1995).

The sample seismograms studied here generally have a more complex spectral content at the beginning than in the coda. In many cases, the time–frequency analysis identifies, near the signal onset, arrivals of relatively short-duration seismic phases with energy concentration in a narrow spectral band. The frequency of this band is either higher (Galeras and Kelut events) or lower (Purace and Misti events) than the main resonance frequency which dominates the coda. Furthermore, in the case of the events at the three Andean volcanoes, the waves corresponding to the resonance frequency arrive with delays of several tenths of a second after the first arrivals. A possible interpretation of these observations is that the excitation process, which has its proper characteristic frequency band, generates elastic waves which form part of the first arrivals. The coupling between this process and the resonator produces standing waves which need some time to become established and to radiate waves at the resonance frequency.

The excitation mechanism of the LP events of Galeras, Purace, and Misti is strongly active during a few seconds, rapidly inducing the resonance effect. After this first part of the forcing, the resonance is still sustained by a low-level excitation during tens of seconds, in the same manner as volcanic tremor. This, together with the high Q values of the resonators, explains the long duration of the corresponding seismograms.

The excitation function of the Misti event includes a low-frequency and very short-duration oscillation which produces mainly vertical movements near the crater. The observation of this phase is limited at low frequency by the natural frequency of the 1-Hz seismometer used. More observations of this kind of event with several broadband sensors should produce useful information about the excitation process.

The LP events of Kelut volcano share several features. Their onsets are relatively broadband while their codas are quasi-monochromatic. No significant variations are observed in their dominant frequency within a time scale of up to about 1 day. These LP events may be compared to numerical simulations of the resonance of a fluid-filled crack model (Chouet, 1988). The corresponding synthetic seismograms generally display high-frequency onsets related to the impulsive pressure transient applied as excitation. Their spectra are usually complex, reflecting the excitation of many resonance modes of the rectangular crack. The source resonator of the Kelut events produces very simple spectra, denoting that only one oscillation mode is excited. Although some particular configurations of the fluid-filled crack model can yield quasi-monochromatic signals (Chouet, 1992), other models with a different resonator geometry or with damping mechanisms of the oscillations are also consistent with the observations at Kelut Volcano. For example, a fluid-filled conduit with depth-dependent gas content can produce one dominant spectral peak (Neuberg et al., 2000). In this case of unique oscillation mode, it is easy to analyze the signals and to deconvolve the resonance effects. The resulting residuals are then almost proportional to the excitation functions, plus noise. In the case of the LP events of Kelut Volcano, most of the energy of excitation is at relatively high frequency, compared to the resonance frequency.

The features of the signal obtained by deconvolution of the volcanic tremor at Ruapehu – amplitude variations, broadband spectrum – are consistent with a mechanism of resonator excitation by a white noise signal due, for example, to high-pressure gas flow, as suggested by Hurst (1992) and Hurst and Sherburn (1993). Thus the tremor initiation is probably due to the increase of the excitation process level. The time–frequency analysis of the Ruapehu signal reveals fast fluctuations in its amplitude and frequency content. This observation suggests that the equivalent AR filters are not stationary and that the AR

model and deconvolution of this record are not fully appropriate in this case. Other methods using higher-order representation could be applied to improve the analysis of this kind of signal.

Acknowledgements

We thank Diego Gomez and Roberto Torres of INGEOMINAS (Colombia), Tony Hurst of the Institute of Geological and Nuclear Sciences (New Zealand), Joachim Wassermann of the Institut für Allgemeine und Angewandte Geophysik (Germany), and Jean-Philippe Métaxian of the Institut de Recherches pour le Développement (France) for kindly providing records of LP events and tremor. We are indebted to Bernard Chouet and Takao Ohminato for their detailed reviews.

References

Adnet, C., 1990. Unification des méthodes d'analyse spectrale (Fourier et haute résolution) en vue de la réalisation d'un système expert d'aide à l'analyse. Ph.D. Thesis, INPG, Grenoble.

Aki, K., Fehler, M., Das, S., 1977. Source mechanism of volcanic tremor: fluid-driven crack models and their implication to the 1963 Kilauea eruption. J. Volcanol. Geotherm. Res. 2, 259–287.

Bellanger M., 1981. Traitement numérique du signal. Masson, Paris.

Brüstle, W., 1991. Signal characteristics of volcanic tremor during change from low to high activity. In: Schick, R., Mugiono, R. (Eds.), Volcanic Tremor and Magma Flow. Forschungszentrum, Jülich, pp. 5–29.

Capon, J., 1972. High-resolution frequency-wavenumber spectrum analysis. Proc. IEEE 37, 1048–1418.

Chouet, B., 1981. Ground motion in the near field of a fluid-driven crack and its interpretation in the study of shallow volcanic tremor. J. Geophys. Res. 86, 5985–6016.

Chouet, B., 1985. Excitation of a buried magmatic pipe: A seismic source model for volcanic tremor. J. Geophys. Res. 90, 1881–1893.

Chouet, B., 1986. Dynamics of a fluid-driven crack in three dimensions by the finite difference method. J. Geophys. Res. 91, 13,967–13,992.

Chouet, B., 1988. Resonance of a fluid-driven crack: radiation properties and implications for the source of long-period events and harmonic tremor. J. Geophys. Res. 93, 4375–4400.

Chouet, B., 1992. A seismic model for the source of long-period events and harmonic tremor. In: Gasparini, P., Scarpa, R., Aki, K. (Eds.), Volcanic Seismology. Springer-Verlag, Berlin, pp. 133–156.

Chouet, B., Page, R.A., Stephens, C.D., Lahr, J.C., Power, J.A., 1994. Precursory swarms of long-period events at Redoubt volcano (1989–1990), Alaska: Their origin and use as a forecasting tool. J. Volcanol. Geotherm. Res. 62, 95–135.

Chouet, B., 1996a. Long-period volcano seismicity: its source and use in eruption forecasting. Nature 380, 309–316.

Chouet, B., 1996b. New methods and future trends in seismological volcano monitoring. In: Scarpa, R., Tilling, R.I. (Eds.), Monitoring and Mitigation of Volcano Hazards. Springer-Verlag, Berlin, pp. 23–97.

Coppens, F., Mari, J.-L., 1984. L'égalisation spectrale: un moyen d'améliorer la qualité des données sismiques. Geophys. Prospect. 32, 258–281.

Crosson, R.S., Bame, D.A., 1985. A spherical source model for low frequency volcanic earthquake. J. Geophys. Res. 90, 10,237–10,247.

Daubechies, I., 1990. The Wavelet Transform, time-frequency localisation and signal analysis. IEEE Trans. Info. Theor. 36, 961–1005.

Feng Chao, B., Gilbert, F., 1980. Autoregressive estimation of complex eigenfrequencies in low frequency seismic spectra. Geophys. J. R. Astron. Soc. 63, 641–657.

Fernandez, J., Martin, N., 1986. Adaptive spectral estimation by ML filtering. EUSIPCO-86, Signal Processing III, Theories and Applications, The Hague, pp. 323–326.

Ferrick, M.G., Qamar, A., St. Lawrence, W.F., 1982. Source mechanism of volcanic tremor. J. Geophys. Res. 87, 8675–8683.

Flandrin, P., Martin, N., Basseville, M., 1992. Méthodes temps-fréquence. Suppl. Trait. Signal 9, 77–147.

Fujita, E., Ida, Y., Oikawa, J., 1995. Eigen oscillation of a fluid sphere and source mechanism of harmonic volcanic tremor. J. Volcanol. Geotherm. Res. 69, 365–378.

Fukao, Y., Suda, N., 1989. Core modes of the Earth's free oscillations and structure of the inner core. Geophys. Res. Lett. 16, 401–404.

Garcés, M.A., McNutt, S.R., 1997. Theory of the airborne sound field generated in a resonant magma conduit. J. Volcanol. Geotherm. Res. 78, 155–178.

Gómez, D.M., Torres, R.A., 1997. Unusual low-frequency volcanic seismic events with slowly decaying coda waves observed at Galeras and other volcanoes. J. Volcanol. Geotherm. Res. 77, 173–193.

Gordeev, E., 1993. Modeling of volcanic tremor as explosive point sources in a single-layered, elastic half-space. J. Geophys. Res. 98, 19,687–19,703.

Goupillaud, P., Grossman, A., Morlet, J., 1984. Cycle octave and related transforms in seismic signals analysis. Geoexploration 23, 85–102.

Harris, F.J., 1978. On the use of windows for harmonic analysis with the discrete Fourier transform. Proc. IEEE 66, 51–83.

Hurst, A.W., 1992. Stochastic simulation of volcanic tremor from Ruapehu. J. Volcanol. Geotherm. Res. 51, 185–198.

Hurst, A.W., Sherburn, S., 1993. Volcanic tremor at Ruapehu:

characteristics and implications for the resonant source. N.Z. J. Geol. Geophys. 36, 475–485.

Julian, B.R., 1994. Volcanic tremor: nonlinear excitation by fluid flow. J. Geophys. Res. 99, 11,859–11,877.

Kay, S.M., Marple, S.L., 1981. Spectrum analysis – A modern perspective. Proc. IEEE 69, 1380–1419.

Kedar, S., Kanamori, H., Sturtevant, B., 1998. Bubble collapse as the source of tremor at Old Faithful Geyser. J. Geophys. Res. 103, 24,283–24,299.

Kumagai, H., Chouet, B.A., 1999. The complex frequencies of long-period seismic events as probes of fluid composition beneath volcanoes. Geophys. J. Int. 138, F7–F12.

Kumagai, H., Chouet, B.A., 2000. Acoustic properties of a crack containing magmatic or hydrothermal fluids. J. Geophys. Res. 105, 25,493–25,512.

Kumar, P., Foufoula-Georgiou, E., 1997. Wavelet analysis for geophysical applications. Rev. Geophys. 35, 385–412.

Lacoss, R.T., 1971. Data adaptative spectral analysis methods. Geophysics 36, 661–675.

Lagunas-Hernandez, M.A., Gasull-Llampadas, A., 1984. An improved maximum likelihood method for power spectral density estimation. Proc. IEEE, Trans. Acoust. Speech Signal Process. 32, 1.

Leet, R.C., 1988. Saturated and subcooled hydrothermal boiling in groundwater flow channels as a source of harmonic tremor. J. Geophys. Res. 93, 4835–4849.

Lesage, P., Mora, M., Dorel, J., Alvarado, G., Métaxian, J.-Ph., 1999. A Study of Tremor and LP Events at Arenal Volcano, Costa Rica. First Results of a Seismic Experiment using Small Aperture and Radial Arrays. Internationa; Union of Geodesy and Geophysics, Birmingham.

Lesage, P., Surono, 1995. Seismic precursors of the February 10, 1990 eruption of Kelut volcano, Java. J. Volcanol. Geotherm. Res. 65, 135–146.

Lu, N.Q., Prosperetti, A., Yoon, S.W., 1990. Underwater noise emissions from bubble clouds. IEEE J. Ocean. Eng. 15, 275–281.

Mallat, S., 1989. A theory for multiresolution signal decomposition: The wavelet representation. IEEE Trans. Pat. Anal. Machine Intell. 11, 674–693.

Mari, J.-L., Glangeaud, F., Coppens, F., 1998. Signal Processing for Geologists and Geophysicists. Technip, Paris.

Marple, S.L., 1987. Digital Spectral Analysis with Applications. Prentice Hall, New York.

Meyer, Y., 1989. Orthonormal wavelets. In: Combes, J.M., Grossman, A., Tchamitchian, Ph. (Eds.), Wavelets Time Frequency Methods and Phase Space. Springer-Verlag, Berlin.

Mora, M., Lesage, Ph., Dorel, J., Bard, P.-Y., Métaxian, J.-Ph., Alvarado, G.E., Leandro, C., 2001. Study of seismic site effects using H/V spectral ratios at Arenal Volcano, Costa Rica. Geophys. Res. Lett. 28, 2991–2994.

Morlet, J., Arens, G., Fourgeau, E., Giard, D., 1982. Wave propagation and sampling theory, part I and II. Geophysics 47, 203–236.

Morrissey, M.M., Chouet, B.A., 1997. A numerical investigation of choked flow dynamics and its application to the triggering mechanism of long-period events at Redoubt volcano, Alaska. J. Geophys. Res. 102, 7965–7983.

Nakano, M., Kumagai, H., Kumazawa, M., Yamaoka, K., Chouet, B., 1998. The excitation and characteristic frequency of the long-period volcanic event: an approach based on an inhomogeneous autoregressive model of a linear dynamic system. J. Geophys. Res. 103, 10,031–10,046.

Neuberg, J., Luckett, R., Baptie, B., Olsen, K., 2000. Models of tremor and low-frequency earthquake swarms on Montserrat. J. Volcanol. Geotherm. Res. 101, 83–104.

Nguyen, M.Q., Glangeaud, F., Mars, J., 1999. Mixed surface elimination, 61st Meeting of European Association of Geophysicists and Engineers, Helsinki, Expanded Abstract.

Oppenheim, A.V., Schafer, R.W., 1975. Digital Signal Processing. Prentice Hall, New York.

Seidl, D., Kirbany, S.B., Brüstle, W., 1990. Maximum entropy spectral analysis of volcanic tremor using data from Etna (Sicily) and Merapi (central Java). Bull. Volcanol. 52, 460–474.

Yoon, S.W., Crum, L.A., Prosperetti, A., Lu, N.Q., 1991. An investigation of the collective oscillations of a bubble cloud. J. Acoust. Soc. Am. 89, 700–706.